

# Nonclassical Transport and Particle-Field Coupling: from Laboratory Plasmas to the Solar Wind

D. Perrone · R.O. Dendy · I. Furno · R. Sanchez ·  
G. Zimbardo · A. Bovet · A. Fasoli · K. Gustafson ·  
S. Perri · P. Ricci · F. Valentini

Received: 30 October 2012 / Accepted: 30 January 2013 / Published online: 8 March 2013  
© Springer Science+Business Media Dordrecht 2013

**Abstract** Understanding transport of thermal and suprathermal particles is a fundamental issue in laboratory, solar-terrestrial, and astrophysical plasmas. For laboratory fusion experiments, confinement of particles and energy is essential for sustaining the plasma long enough to reach burning conditions. For solar wind and magnetospheric plasmas, transport properties determine the spatial and temporal distribution of energetic particles, which can be harmful for spacecraft functioning, as well as the entry of solar wind plasma into the magnetosphere. For astrophysical plasmas, transport properties determine the efficiency of particle acceleration processes and affect observable radiative signatures. In all cases, transport depends on the interaction of thermal and suprathermal particles with the electric and magnetic fluctuations in the plasma. Understanding transport therefore requires us to understand these interactions, which encompass a wide range of scales, from magnetohydrodynamic to kinetic scales, with larger scale structures also having a role. The wealth of transport studies during recent decades has shown the existence of a variety of regimes that differ from the classical quasilinear regime. In this paper we give an overview of nonclassical plasma transport regimes, discussing theoretical approaches to superdiffusive and subdiffusive transport, wave–particle interactions at microscopic kinetic scales, the influence of coherent structures

---

D. Perrone (✉) · G. Zimbardo · S. Perri · F. Valentini  
Department of Physics, University of Calabria, Ponte P. Bucci, Cubo 31C, 87036 Rende, Italy  
e-mail: [denise.perrone@fis.unical.it](mailto:denise.perrone@fis.unical.it)

R.O. Dendy  
Culham Science Centre, Euratom/CCFE Fusion Association, Abingdon, Oxfordshire OX14 3DB, UK

R.O. Dendy  
Centre for Fusion, Space and Astrophysics, Department of Physics, Warwick University, Coventry CV4 7AL, UK

I. Furno · A. Bovet · A. Fasoli · K. Gustafson · P. Ricci  
Centre de Recherches en Physique des Plasmas (CRPP), Ecole Polytechnique Fédérale de Lausanne (EPFL), Association Euratom-Suisse, 1015 Lausanne, Switzerland

R. Sanchez  
Department of Physics, Universidad Carlos III, Leganés 28911, Madrid, Spain

and of avalanching transport, and the results of numerical simulations and experimental data analyses. Applications to laboratory plasmas and space plasmas are discussed.

**Keywords** Transport · Wave–particle interaction · Laboratory plasmas · Space plasmas · Anomalous diffusion

## 1 Introduction

This paper addresses the problems of nonclassical, nondiffusive transport and of the coupling between particles and fields on an extended range of scales. We give an overview of these problems in laboratory plasmas and in space and astrophysical plasmas, and examine the inter-relationships, with the aim of assisting the exchange of novel ideas and techniques. In magnetized, nearly collisionless plasmas, the main contribution to transport comes from the influence of electric and magnetic turbulence on the particle motion, either in the form of drift velocities perpendicular to the background magnetic field, or because of resonant effects such as pitch-angle scattering, or because of the field-line random walk due to low frequency magnetic fluctuations. In addition, if turbulence influences transport, then transport influences the equilibrium plasma structure and hence dynamical processes such as particle acceleration that may depend on this structure. Plasma fluid or kinetic instabilities can modify the spectrum of electromagnetic fluctuations, for example by means of a nonlinear cascade, feeding further energy into turbulence. Thus, a complex coupling between plasma turbulence and transport, combining fluid and kinetic properties, arises. Due to the complexity of the problem, transport is sometimes considered from a test-particle perspective, as distinct from a fully self-consistent treatment. In the last two decades, a number of transport regimes different from the classical quasilinear regime have gained increasing attention. These include anomalous transport regimes including subdiffusion and superdiffusion (Zumofen et al. 1989), diffusive but non-quasilinear regimes such as percolation (e.g., Zimbaro et al. 2000a, 2012), and avalanching transport as well as the influence of coherent structures. Due to the broadness of these topics, we do not give a systematic coverage of the fields of transport and wave–particle interactions, but rather highlight a number of current approaches.

The topics addressed in this review all illustrate the fact that space and laboratory plasmas are complex systems in the technical sense (Dendy et al. 2007). That is, their phenomenology is governed by the interaction of multiple physical processes, each of which operates within a distinct range of length scales and time scales. These processes are nonlinearly coupled, and together span a very wide dynamic range. As an example, let us consider a plasma environment which is characterized by the presence of suprathermal particles, i.e. with energy larger than characteristic bulk plasma temperatures, possibly generated by turbulent acceleration, external sources, or, in the case of fusion devices, nuclear reactions. Understanding the nature of the transport of suprathermal particles is a key challenge for the description of a wide range of plasma systems, ranging from magnetically confined plasmas for fusion to space plasmas. In particular, this subject is receiving much attention in fusion research since, in future fusion reactors, additional heating will be needed to reach the burning regime, which will create strong suprathermal ion components, for example via the injection of energetic neutral beams (NBI). When burning conditions are reached, the majority of the heating will come from the fusion-generated, highly-energetic alpha particles. Good confinement of the slowing-down alpha particles and of the NBI-generated fast ions is therefore crucial. Despite its importance, the interaction between highly energetic ions

and small-scale turbulence has not been extensively investigated to date. One of the reasons is that, in present fusion devices, suprathermal ions do not play a crucial role. The other more fundamental reason is that, as the suprathermal ions usually have a gyroradius that is larger than the turbulence scale, their interaction with turbulence is expected to be relatively weak. Gyro-averaging effects would then weaken or almost entirely suppress the interaction of alphas with turbulence, leading to subdiffusive transport. However, the question of how complete this suppression becomes in different regimes is still open. In addition, the results in Günter et al. (2005) indicate that a significant redistribution of suprathermal ions can be induced by turbulence. So far, no direct measurements of fluctuation induced fast-ion transport in toroidal devices have been performed. Thus there exists a strong need for experimental data with which to compare and validate the relevant theoretical models and numerical simulations. For these reasons, theoretical and experimental studies of suprathermal ion transport in turbulent plasmas are currently operating on basic plasma physics experiments, which allow a relatively simple experimental environment with easy access for diagnostics and well established plasma scenarios. In this review, among other examples, we will describe experimental and theoretical efforts to understand suprathermal particle transport in the TORPEX device (Fasoli et al. 2006, 2010).

In the solar wind, understanding transport is important for predicting the arrival of solar energetic particles (SEP) from the sun—one of the main concerns of space weather—and for understanding how, when, and where solar wind plasma enters the magnetosphere. The observation of non-thermal, non-isotropic particle distribution functions in the solar wind calls for a better understanding of wave–particle interactions and pitch-angle diffusion, possibly in a nonlinear regime. Further, the transport properties influence cosmic ray acceleration processes, notably diffusive shock acceleration. Both numerical and analytical studies show transport depends both on magnetic fluctuation level and on the turbulence anisotropy (Pommois et al. 1999; Zimbaro 2005). Here, too, the wave–particle interaction depends on the gyroradius, so that a number of different transport regimes are obtained.

The organization of this review is as follows: in Sect. 2, we discuss the theoretical framework appropriate to describe nondiffusive transport, emphasizing the presence of long-range correlation and non-Gaussian statistics. Concepts such as the continuous-time random walk (CTRW) and fractional diffusion equations are briefly introduced. In Sect. 3 we describe the study of wave–particle interactions by means of kinetic Vlasov simulations: such self-consistent studies gives information on small scale turbulence dissipation and on pitch angle scattering in the nonlinear regime. In Sect. 4, the effect of finite Larmor radius is investigated with regard to transport in laboratory and solar wind plasmas. We discuss results from Vlasov simulations and test-particle simulations, where both subdiffusive and superdiffusive regimes are found in many cases. Section 5 addresses the interaction between particle physics on the ion gyroscale, small-scale turbulence which may retain features of underlying linear wave physics, and larger-scale coherent nonlinear structures. In a typical laboratory plasma, this involves coupled physics unfolding over three orders of magnitude in length scale, and many more in time scale. Section 6 deals with avalanching transport, which typically arises (Dendy and Hellander 1997) in physical systems where correlation exists on all length scales, leading to scale-free phenomenology and non-Gaussian fluctuation statistics and emitted signals (Dendy and Chapman 2006). In Sect. 7 we briefly discuss how the extension of diffusive shock acceleration (the standard model for the acceleration of cosmic rays) (Fisk and Lee 1980; Lee and Fisk 1982) to the case of superdiffusion leads to a new expression for the energy spectral index of accelerated particles. In Sect. 8 we give our conclusions.

## 2 Overview of Novel Transport Regimes

In nature, many systems exhibit complex and non-diffusive behavior. These systems usually share the characteristics of having many degrees of freedom that interact dominantly via nonlinear interactions, and in an environment that fosters self-organization, memory effects, long-range correlations, and non-diffusive transport. By non-diffusive transport, we mean transport processes in which fluxes are not trivially related to the local instantaneous values of the gradients of the transported fields; instead a more complicated relation exists between these quantities, which can include non-local kernels both in space and time. These types of transport behavior have been observed both in space and laboratory plasmas, and a substantial effort has been made to characterize these regimes and understand the physical mechanisms that cause them. Examples are provided by the dynamics of solar flares (Lu and Hamilton 1991), magnetic substorms in Earth's magnetosphere (Klimas et al. 2000), and radial turbulent transport in fusion devices and basic plasma experiments (Carreras et al. 1996; Newman et al. 1996; Fasoli et al. 2010) to name just a few.

### 2.1 Propagators of Non-diffusive Transport Equations

Many ways exist to characterize the complexity of transport. A relatively simple technique is to define the Green function (or *propagator*) of the effective equation characterizing the transport process. Say, for instance, that we consider the standard diffusive transport equation in one-dimension:

$$\frac{\partial n}{\partial t} = D \frac{\partial^2 n}{\partial x^2}. \quad (1)$$

The propagator of this equation is provided by the temporal evolution of the initial condition  $n(x, 0) = \delta(x - x_0)$ . It is well known that this Green function is  $n(x, t) = G((x - x_0)/\sqrt{2Dt})$ , where  $G(x)$  is the standard Gaussian distribution. Thus, the propagator is just a Gaussian function whose variance increases linearly with time. This behavior is usually called *diffusive transport*. However, in many cases it is possible to measure these propagators directly: for example, by following the evolution in time of a spatially localized initial concentration of a tracer population. This means that we do not need to assume any form for the transport equation in advance. In some cases, the inferred propagator is not a Gaussian with a variance that grows linearly in time. Sometimes the variance of the propagator, although corresponding to a Gaussian distribution, increases faster than linear (i.e.,  $\sigma^2 \propto t^{2H}$ ,  $H > 1/2$ ). We call this behavior *superdiffusive transport*. In other cases,  $\sigma^2 \propto t^{2H}$ ,  $H < 1/2$ , and we speak of *subdiffusion*.

Another frequent occurrence in practice is that the shape of the observed propagator is non-Gaussian. The central limit theorem, which lies at the heart of why Gaussian distributions are so frequently exhibited by physical processes, also provides alternative stable distributions in the case where some of its assumptions are relaxed. For instance, if one relaxes the constraint of having a finite variance, the central limit theorem yields the so-called *Lévy distributions* as the limiting distribution of the sum of stochastic processes (Samorodnitsky and Taqqu 1994). In the case of symmetry with respect to  $x$ , Lévy distributions can be simply expressed as the inverse Fourier transform of their characteristic function,  $\exp(-C|k|^\alpha)$ , where  $C$  is a scale parameter (e.g., Zaslavsky 2002). Clearly, for  $\alpha = 2$  we recover a Gaussian, while for  $\alpha < 2$  Lévy laws decay algebraically as  $|x|^{-(1+\alpha)}$ , with  $\alpha \in (0, 2)$ , instead of exponentially as Gaussians do. Lévy laws are usually a signature of the existence of transport via avalanching processes, non-local interactions, and long-range correlations, whose

characteristic size is not set by the underlying physical process, but by the size of the system instead. This causes the divergence of the variance of the propagator. The empirical identification of propagators corresponding to this class of distributions with fat tails—that is an excess of large events compared to Gaussian—is usually a signature of non-diffusive, avalanche-driven transport.

The transport exponents  $\alpha$  and  $H$  are very useful to characterize transport. Their diffusive values are  $\alpha = 2$  and  $H = 1/2$ , but values in the range  $\alpha \in (0, 2]$  and  $H \in (0, 2]$  are possible. The physical meaning of these exponents is rather different. In particular,  $\alpha$  can be related to the statistics of the underlying microscopic displacements that cause the overall motion, in a view reminiscent of the random-walk or Langevin descriptions (Sanchez et al. 2006). On the other hand,  $H$  is related to the correlation or memory existent in the transport process. For instance, for  $H < 1$ , the exponent  $\beta = \alpha H$  is such that  $\beta = 1$  implies a Markovian microscopic process. Here,  $\beta$  appears in the exponent of the waiting time power-law distribution, see below conversely  $\beta < 1$  implies that the underlying microscopic transport process is non-Markovian, at least in a Lagrangian way (Sanchez et al. 2006).

Several propagators of effective transport equations based on fractional differential equations, see below, are known either analytically or from series expansions (Mainardi et al. 1996; del-Castillo-Negrete et al. 2004b; Sanchez et al. 2008). Comparison between these and empirically inferred propagators can help identify the best fractional transport equation for a particular system.

## 2.2 Lagrangian Statistics and Correlations

There are other ways to measure the transport exponents, in addition to constructing the propagators. For instance, when one has access to Lagrangian information concerning the transport process (say, via tracer trajectories), it can be shown that  $\alpha$  can be obtained from the statistics of the Lagrangian displacements, whilst  $H$  can be obtained from the temporal correlation of their ordered time series (Mier et al. 2008). Also called the Hurst exponent in this context,  $H$  can be obtained by many different techniques such as the R/S rescaled range analysis (e.g., Feder 1988), or the detrended fluctuation analysis among other methods (Dendy and Chapman 2006).

It is also possible to relate these exponents to the correlation function of the Lagrangian velocities or displacements,  $C_L(\tau) \equiv \langle v(t)v(t + \tau) \rangle$ , where the angle bracket refers to an ensemble average over Lagrangian trajectories. A homogeneous system is usually assumed, so that the correlation function depends only on the time delay  $\tau$ . In the diffusive case, this function is related to the effective diffusivity of the process via the Taylor-Green-Kubo (TGK) relation (e.g., Shalchi 2011),

$$D = \int_0^\infty C_L(\tau) d\tau. \tag{2}$$

It is also possible to infer from this relation when super- or sub-diffusion may occur depending on the velocities correlation function. Superdiffusion occurs if  $C_L(\tau)$  is not integrable, which requires that

$$C_L(\tau) \sim \tau^{-2(1-H)} \tag{3}$$

for large  $\tau$  (Mandelbrot and van Ness 1968). Here we have purposely expressed the power-law in terms of the Hurst exponent. Since  $H > 1/2$  for superdiffusion, it follows that the integral in Eq. (2) diverges, corresponding to the presence of long range correlations. On the

other hand, subdiffusion requires that  $H < 1/2$ , which ensures that the integral in the TGK relation is finite. However, a finite value would imply diffusive behavior, and it therefore follows that the integral of  $C_L(\tau)$  must be exactly zero to yield subdiffusion. This implies that the long-time behavior of the autocorrelation function, although correctly given by the previous scaling in terms of the Hurst exponent, must be negative. This is a consequence of the negative correlation that is always responsible for subdiffusive behavior. Indeed, it can be shown (e.g., Feder 1988) that for  $H \neq 1/2$  the probability of past and future Lagrangian displacements  $\Delta x_i$  is correlated, that is for  $H > 1/2$  positive increments in the past imply positive increments in the future—this is called a persistent process. Conversely, for  $H < 1/2$  a positive increment in the past implies a negative increment in the future—this is an antipersistent process.

In the case where the statistics of the Lagrangian velocities are Lévy-like (and characterized with some exponent  $\alpha$ , as we mentioned before), the TGK relation breaks down: the integral diverges for any value of  $H$  due to the lack of a finite variance of the statistics of the velocities. In a spatiotemporally finite system, however, the correlation function is still meaningful, and many of the preceding statements remain valid, although  $C_L(\tau)$  will non-trivially scale with the size of the system (Sanchez et al. 2006). It is however important to note, in that case, and for a finite system,

$$C_L(\tau) \sim \tau^{-(2-\alpha H)}. \quad (4)$$

### 2.3 Continuous-Time Random Walk Model

Yet another, particularly transparent and easily generalizable, microscale approach to describe the spreading of a population of particles is the continuous-time random walk (CTRW) (Montroll and Weiss 1965). This approach consists of following the trajectories of particles, the random walkers, through a sequence of steps. The CTRW is defined by  $\phi(\Delta \mathbf{r}, \Delta t)$ , which is the probability distribution function (PDF) for a random walker to make a step of length  $\Delta \mathbf{r}$  that takes a time  $\Delta t$ . The time taken to make a step is also called the waiting time, because of models where the random walk is described as a consequence of instantaneous jumps separated by a time  $\Delta t$ . In the simplest (and initial) formulation, homogeneity in space and time is assumed, as well as separability of the jumping and waiting processes. This means that

$$\phi(\Delta \mathbf{r}, \Delta t) = p(\Delta \mathbf{r}) \cdot \psi(\Delta t), \quad (5)$$

where  $p$  is known as the step-size distribution, and  $\psi$  as the waiting time distribution. We note that it is not difficult to remove these constraints from the CTRW formulation (Shugard and Reiss 1976; van Milligen et al. 2004). As shown by Montroll and Weiss (1965), the probability distribution  $\phi(\Delta x, \Delta t)$  allows one to compute the time behavior of the mean-square derivation by inserting the Fourier-Laplace transform  $\widehat{\phi}$  into the Fourier-Laplace transform of the propagator  $P(x, t)$ , as given by the Montroll-Weiss equation (e.g., Ragot and Kirk 1997)

$$\widehat{P}(k, s) = \frac{1 - \widetilde{\psi}(s)}{s} \frac{1}{1 - \widehat{\phi}(k, s)}. \quad (6)$$

Standard diffusive transport is recovered from the CTRW in the limit of long times and large distances, if  $p$  and  $\phi$  have finite mean and variances. This limit is exact if  $p$  is a Gaussian law, and  $\psi$  an exponential. However, non-diffusive transport is exhibited by this simple

CTRW realization if  $p$  is chosen to follow a power-law distribution known as a Lévy law. Lévy laws are characterized by one exponent  $0 < \alpha \leq 2$  that defines the asymptotic behavior of the distribution:  $p(\Delta x) \sim |\Delta x|^{-(1+\alpha)}$ , for large argument. Here, we have assumed one-dimensionality for simplicity. This asymptotic behavior guarantees a divergent variance for the distribution of step-sizes. Similarly, for the waiting-time distribution it is a requirement that  $\psi(\Delta t) \sim (\Delta t)^{-(1+\beta)}$  for large argument, where  $0 < \beta \leq 1$ . Again, this guarantees a divergent mean waiting-time. A Gaussian  $p$  is recovered in the case  $\alpha > 2$ , and an exponential is recovered when  $\beta \rightarrow 1$  (Samorodnitsky and Taqqu 1994).

The separable CTRW model is very useful for analyzing real transport situations. It can be implemented by collecting sufficient statistics of step-sizes and waiting-times from the motion of a population of particles or tracers. However is not always straightforward to come up with a reasonable definition of what a step-size and a waiting-time should be. Indeed, there are many cases in which particles are never at rest, for instance, when advected by turbulence. It is then a question of intuition to choose these quantities correctly (e.g., Zimbaro et al. 2000b). Assuming this is done appropriately, it is straightforward to show that the variance of the distribution of the tracers scales as:

$$\sigma^2 \sim t^{2H}, \quad H = \beta/\alpha. \tag{7}$$

The transport exponent  $H$  again tells us whether diffusive ( $H = 1/2$ ), superdiffusive ( $H > 1/2$ ) or subdiffusive ( $H < 1/2$ ) transport takes place in the system.

It is also interesting to note that, in the long-time, large-distance limit, the CTRW can be shown to be well represented by the following transport equation under very general conditions (Sanchez et al. 2005),

$$\frac{\partial^\beta n}{\partial t^\beta} = D \frac{\partial^\alpha n}{\partial |x|^\alpha}, \tag{8}$$

where the fractional derivatives require introduction. Fractional derivatives are a class of integro-differential operators, which can be defined in a number of ways (e.g., del-Castillo-Negrete et al. 2004a; Sanchez et al. 2005). The Riemann-Liouville definition is

$$\frac{\partial^\mu \phi(x, t)}{\partial x^\mu} = {}_a D_x^\mu \phi(x, t) = \frac{1}{\Gamma(m - \mu)} \frac{\partial^m}{\partial x^m} \int_a^x \frac{\phi(x', t)}{(x - x')^{1+\mu-m}} dx' \tag{9}$$

and

$$\frac{\partial^\mu \phi(x, t)}{\partial (-x)^\mu} = {}^b D_x^\mu \phi(x, t) = \frac{(-1)^m}{\Gamma(m - \mu)} \frac{\partial^m}{\partial x^m} \int_x^b \frac{\phi(x', t)}{(x' - x)^{1+\mu-m}} dx' \tag{10}$$

where  $m - 1 < \mu < m$ , with integer  $m$ . The symmetric Riesz fractional derivative, used in the rhs of Eq. (8) above, is given by

$$\frac{\partial^\alpha}{\partial |x|^\alpha} = -\frac{1}{2 \cos(\pi\alpha/2)} [{}_{-\infty} D_x^\alpha + {}^\infty D_x^\alpha]. \tag{11}$$

Fractional derivatives reduce to ordinary ones when  $\mu$  is integer, while their integral form makes them an appropriate tool to study non-local phenomena, long range correlations, and scale-free transport. In fact, propagators for this family of equations (8) are known (Mainardi et al. 1996), and this connects the CTRW approach with the transport exponents  $\alpha$  and  $\beta$

described in Sect. 2.1. For instance, use of the Riesz fractional derivative in Eq. (8), for  $\beta = 1$  leads to a Fourier transform of the form

$$\frac{\partial \widehat{n}(k)}{\partial t} = -D|k|^\alpha \widehat{n}(k) \quad (12)$$

whose solution is the characteristic function of a Lévy distribution.

A commonly used non-Gaussian CTRW based on a probabilistic description involving a Lévy random walk was introduced by Klafter et al. (1987). The difference from the CTRW just described is that here, in the random walk of single particles of a given constant energy, a large displacement  $\Delta x$  is associated with a correspondingly long time  $\Delta t \equiv \Delta x/v$ . Then, in one dimension, the probability  $\phi$  of a random walker making a free path of length  $\Delta x$  (forward or backward) in a time  $\Delta t$  is given as

$$\phi(\Delta x, \Delta t) = A|\Delta x|^{-(1+\alpha)} \delta(\Delta x - v\Delta t), \quad |\Delta x| > \Delta x_0. \quad (13)$$

Here it is important to have coupling between free path length and free path duration, as expressed by the delta function, in order to ensure the conservation of the particle energy, i.e. constant velocity (note that Klafter et al. (1987) uses instead the notation  $\mu \equiv 1 + \alpha$ ). The constant velocity requirement may however be relaxed when considering, for instance, the  $\delta \mathbf{E} \times \mathbf{B}$  drift velocity induced by electric fluctuations if  $\delta \mathbf{E}$  is a stochastic quantity. For  $|\Delta x| < \Delta x_0$ , a regular bell-shaped distribution of  $\phi$  is assumed. For  $\alpha < 2$  in Eq. (13) (i.e., a Lévy law), the mean square value of  $\Delta x$ , and hence the mean free path  $\lambda$ , is divergent:

$$\langle \Delta x^2 \rangle = \int \Delta x^2 \phi(\Delta x, \Delta t) d\Delta x d\Delta t \rightarrow \infty, \quad \alpha < 2. \quad (14)$$

This means that the central limit theorem, which leads to normal diffusion for finite  $\langle \Delta x^2 \rangle$ , requires instead a Lévy distribution for the propagator, and the normal diffusion coefficient is divergent. Therefore, this CTRW for  $\alpha < 2$  represents another way to describe anomalous transport. By inserting Eq. (13) into Eq. (6), it can be shown that the transport regime depends on the index  $\alpha$  of the free path probability distribution,

$$\sigma^2(t) \propto \begin{cases} t^2 & 0 < \alpha < 1, \\ t^{3-\alpha} & 1 < \alpha < 2, \\ t & \alpha > 2 \end{cases} \quad (15)$$

so that superdiffusion with  $H = (3 - \alpha)/2$  is obtained for  $1 < \alpha < 2$  (Klafter et al. 1987). For  $\alpha < 1$ , ballistic transport is obtained; for  $\alpha > 2$ , standard diffusion.

## 2.4 Examples

In the previous subsections we have discussed several possible nondiffusive behaviors, including both subdiffusion and superdiffusion, as well as several models useful to diagnose their presence in practical situations. In this subsection, we describe several examples in which these non-diffusive dynamics are present.

We start with subdiffusive transport which, as mentioned, requires the existence of antipersistent correlations. It is interesting to note that one natural and important case of antipersistent correlations is found for plasma transport perpendicular to the average magnetic field, when either collisions or pitch-angle scattering cause diffusive motion along the magnetic field, i.e.,  $\sigma_z^2 = 2D_{\parallel} t$ . In the presence of magnetostatic fluctuations, the magnetic field

lines may diffuse in the perpendicular direction as  $\sigma_{\perp}^2 = 2D_m \Delta z$ , and the resulting perpendicular particle transport is (Rechester and Rosenbluth 1978)

$$\sigma_{\perp}^2 = 2D_m \sqrt{2D_{\parallel} t}, \tag{16}$$

which clearly is subdiffusive in time. This transport regime is called double diffusion in laboratory plasmas (Krommes et al. 1983) and compound diffusion in astrophysical plasmas (Duffy et al. 1995; Kóta and Jokipii 2000; Zimbardo et al. 2009; Bitane et al. 2010; Hornsby et al. 2010), and corresponds to  $H = 1/4$ . Physically, the antipersistence is due to the fact that pitch angle scattering forces particles to trace back the magnetic field lines (in the magnetostatic case), so that a positive perpendicular displacement is followed by a negative one.

A further topical example of non-diffusive behavior is the transport of suprathermal ions in a simple magnetized torus (SMT), in which plasmas are confined by a toroidal magnetic field and a smaller vertical component. This magnetic geometry with open helicoidal field lines incorporates the main ingredients for drift and interchange instabilities, namely pressure gradients and magnetic field line curvature. By numerically integrating the trajectories of suprathermal ions in simulated SMT turbulent fields, and by exploring wide ranges of particle energy and turbulence amplitude, it has been recently shown (Gustafson et al. 2012a) that the ions have a complex motion, which in general cannot be considered diffusive. The simulations show that suprathermal ion dispersion in the direction perpendicular to the average magnetic field starts with a brief ballistic phase followed by a turbulence interaction phase, which shows the entire spectrum of suprathermal ion spreading: superdiffusive, diffusive, or subdiffusive, depending on particle energy and turbulence amplitude (Gustafson et al. 2012b).

Other interesting examples can be found in models of cosmic ray acceleration and transport. Recalling normal diffusion implies that the diffusion coefficient  $D$  can be estimated using the TGK relation to yield

$$D = \int_0^{\infty} \langle v_x(0)v_x(t) \rangle dt \approx v_x^2 \tau. \tag{17}$$

Assuming that the mean free path  $\lambda = v\tau$  is given by the mean collision (or correlation) time  $\tau$  times the velocity  $v = (v_x^2 + v_y^2 + v_z^2)^{1/2}$ , we can estimate the diffusion coefficient as  $D \simeq \frac{1}{3}v^2\tau = \frac{1}{3}\lambda v$ . On the other hand, in the case of superdiffusion the above integral diverges. The divergence of  $D$  implies that  $\lambda$  also diverges, since the particle velocity is finite. In particular, for high energy cosmic rays  $v \equiv c$ , so that the constant velocity model of Eq. (13) is appropriate. This property has an immediate impact on models of cosmic ray acceleration and transport, since the mean free path is a fundamental parameter for particle propagation, the acceleration time, and the maximum reachable energy (e.g., Lagage and Cesarsky 1983a, 1983b; Bieber et al. 1994; Reames 1999). The divergence of  $D$  and of  $\lambda$  requires a non Gaussian approach to transport and acceleration in these problems. Some success has been achieved by applying the second CTRW construct introduced in Sect. 2.3, that incorporates a coupling between step-size and waiting-times that depends on the particle velocity (Klafter et al. 1987; Perri and Zimbardo 2012; Gustafson and Ricci 2012; Shlesinger et al. 1982).

### 3 Wave–Particle Interaction at the Kinetic Scales

Thus far we have considered the statistical description of nondiffusive transport. But what are the physical reasons for random particle motions at the microscopic level? In either

weakly collisional or collisionless plasmas, the transport is influenced by electric and magnetic fluctuations and by wave–particle interactions, which cause pitch angle scattering and transverse particle drifts, and by low frequency magnetic fluctuations, which cause field lines to trace a random walk (Jokipii 1966). The strength of these effects varies with the particle species and energy, and with the properties of turbulence, so that a large number of different transport regimes can arise, as shown by independent numerical simulations (Zimbaro et al. 2000a; Pommois et al. 2007; Shalchi and Kourakis 2007; Gustafson et al. 2012b). Detailed study of wave–particle interactions is necessary to understand transport. The portfolio of tools for such study in the kinetic regime has recently been augmented by Vlasov simulations.

In a plasma system where the effects of particle collisions can be considered negligible (such as the solar wind or, in many cases, laboratory plasmas), resonant wave–particle interaction represents the main process by which particles and fields can exchange energy. Wave–particle resonance is central to many physical phenomena including wave damping, particle acceleration, growth of instabilities, generation of anisotropies and, in general, departure from the local thermodynamic equilibrium configuration. In the framework of kinetic theory, the resonant wave–particle interaction is described by the Vlasov equation. In the Vlasov description, complete statistical information about the plasma state is stored in the particle distribution function that represents the probability density in phase space. Analytical solutions of the combined Vlasov–Maxwell equations are known only in a few simplified linear cases, while the nonlinear regime must be investigated numerically.

An important tool to investigate the complexity of the kinetic plasma dynamics is given by the direct numerical simulations. One of the most adopted approaches is represented by the Lagrangian Particle in Cell (PIC) methods (Birdsall and Langdon 1985). Within the PIC approach, the equations of motion of a large number of macroparticles are numerically integrated under the effect of the self-consistent electromagnetic fields. At each time step, the macroscopic plasma variables (density, velocity and current) are obtained by collecting the particles in each grid point of a uniformly spaced grid and then used for the integration of the Maxwell equations for fields. The phase space particle distribution can be evaluated in the same statistically way. In recent years, the PIC codes have been extensively used for the description of the kinetic dynamics of turbulent space plasmas, particularly focusing on many interesting physical aspects, like wave–particle interaction (Araneda et al. 2008), particle heating (Araneda et al. 2009) and turbulence (Gary et al. 2008; Saito et al. 2008; Parashar et al. 2010, 2011; Camporeale and Burgess 2011).

Nowadays, thanks to the impressive increase of the computational technology, the Eulerian approach for the numerical solution of the Vlasov equation has become a valid alternative to the PIC methods. A Eulerian Vlasov code (Mangeney et al. 2002; Valentini et al. 2005, 2007) integrates numerically the Vlasov equation by time-advancing the particle distribution function on a uniform fixed grid in phase space under the effects of the self-consistent electric and magnetic fields. The particle density, the mean velocity and the current density needed for the solution of the Maxwell equations are evaluated at each time step as the velocity moments of the distribution function.

Since the Eulerian Vlasov algorithms advance in time the six-dimensional array that contains the particle distribution function, they are, in many cases, extremely demanding from the point of view of both the execution time and the memory and data storage requirements. However, while in general PIC codes are affected by an intrinsic statistical noise due to the limited number of particles that can be launched in a typical simulation, Eulerian schemes are essentially noise-free. This allows for a clean and precise description of the plasma dynamics even in situations where the PIC results are no longer reliable, like, for example, in

the description of the high energy tails of the particle velocity distributions, in the analyses of low density processes or in the study of the tail at short spatial scales of the solar-wind turbulent cascade, where the energy level of the fluctuations is generally very low.

The numerical description of a Vlasov-Maxwell plasma system requires, in the most general case, to perform simulations in a six-dimensional phase space configuration, for both electrons and ions. Due to the large time scale separation between ion and electron dynamics, full electron-ion Vlasov numerical experiments are out of reach of the presently available computing resources. Nevertheless, significant analyses can be performed in phase space configurations with reduced dimensionality or by focusing on the kinetic dynamics of one particle species at a time. From this latter consideration, the so-called hybrid Vlasov-Maxwell algorithm (Valentini et al. 2007) has been recently developed. Within this hybrid model the Vlasov equation is numerically solved, through a Eulerian scheme, for the ion distribution function, while the electrons are treated as a fluid. Although the kinetic description in this hybrid model is restricted only to the ion species, still the computational cost of the hybrid Vlasov-Maxwell simulations is very high, especially when multi-dimensional problems are treated. For this reason, a massive parallelization procedure, based on the use of the Message Passing Interface (MPI) protocol, has been performed so as to exploit the power of contemporary high performance computation.

In the last years, the Eulerian hybrid Vlasov-Maxwell code has been extensively employed in 1D-3V (one dimension in physical space and three in velocity space) phase space configuration, for the analysis of the kinetic effects on protons during the development of the solar-wind turbulent cascade towards kinetic scales, along the direction of the mean magnetic field (Valentini et al. 2008, 2010, 2011c; Valentini and Veltri 2009). The basic idea behind this numerical research thread is to shed light on the physical mechanisms that replace energy dissipation at short wavelengths in a system, like the solar wind, where collisional viscosity is absent. In this range of short spatial scales, kinetic effects are considered to be the best candidates in governing the system dynamics. Through the analysis of the numerical results of these hybrid Vlasov-Maxwell simulations, a novel branch of electrostatic fluctuations, propagating at a frequency which is a small fraction of the proton plasma frequency, has been identified. These waves, dubbed ion-bulk (IBk) waves (Valentini et al. 2011a, 2011b, 2011c), have acoustic type dispersion and phase velocity comparable to the proton thermal speed. The excitation of these fluctuations was also obtained in laboratory experiments with non-neutral plasmas (Anderegg et al. 2009). At variance with the well-known ion-acoustic waves, the IBk fluctuations can survive against Landau damping (Landau 1946) even for values of the electron to proton temperature ratio of order unity, typical values for the solar-wind environment (as well as for many other plasmas). For these reasons, the IBk fluctuations seem to represent a very efficient channel to carry the solar-wind energy coming from the large MHD scales towards small kinetic scales in the longitudinal component of the energy spectrum.

These hybrid Vlasov-Maxwell simulations have also shown that the resonant interaction of protons with these electrostatic fluctuations produces significant distortions in the longitudinal proton velocity distribution with the generation of a field-aligned beam of accelerated particles that stream at a typical speed close to the local Alfvén velocity. Figure 1(a) displays the longitudinal  $x-v_x$  ( $x$  being the direction of the ambient magnetic field) phase space contour plot of the proton distribution function. This contour plot shows the generation of a localized trapped particle region (delimited by the vertical white dashed lines) moving with mean velocity close to the phase speed of the IBk waves. The presence of this trapped particle population affects the velocity distribution of protons. This is shown in the plot (b) of Fig. 1, where the  $v_x-v_y$  level lines of the proton distribution function, integrated over  $v_z$  and averaged over  $x$  in the spatial region of trapped particles, are reported.

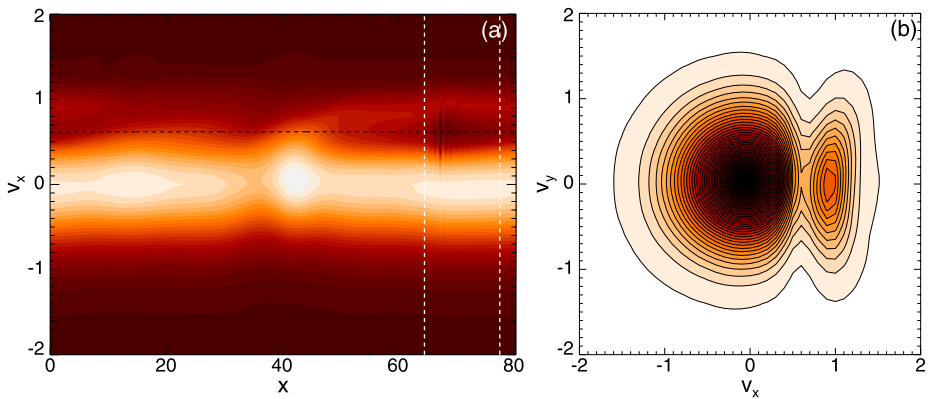


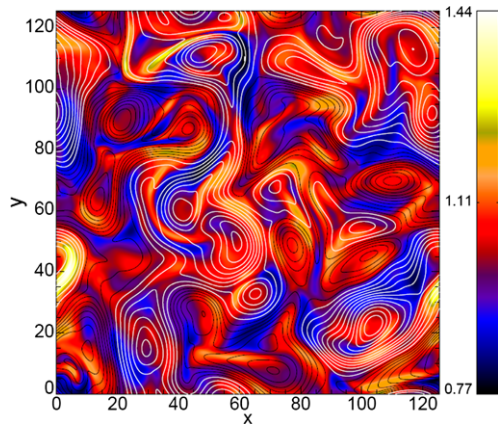
**Fig. 1** (a): Longitudinal  $x-v_x$  phase space contour plot of the proton distribution function. This contour plot displays the generation of localized trapped region. (b): Level lines of proton distribution function in the velocity plane  $v_x-v_y$ . The generation of a well-defined field-aligned beam of protons is recovered (Valentini et al. 2008)

The generation of these double peaked proton velocity distributions has been recovered in many “in situ” spacecraft observations in the solar wind (Gurnett et al. 1979; Marsch et al. 1982a; Marsch 2006). These results show that non-Maxwellian distribution functions with multiple peaks or bumps can be spontaneously created by the wave–particle interactions in the kinetic regime. The generation of field aligned beams means that pitch-angle scattering is not very effective, as it would smooth out the field aligned beams. This shows that a population of particles can propagate along the magnetic field with little or no scattering, thus creating the long “persistent” displacements which are at the basis of the Lévy random walk and superdiffusive transport. Therefore the study of wave–particle interaction can give information on the microphysics of nondiffusive transport regimes.

More recently, the 2D-3V version of the hybrid Vlasov-Maxwell code has been also used to investigate the role of local kinetic effects in plasma turbulence, in the plane perpendicular to an ambient magnetic field (Servidio et al. 2012). In these simulations, during the evolution of turbulence, coherent structures and vortices appear in the bi-dimensional maps of the inplane magnetic field. Nearby the regions of high magnetic stress, magnetic reconnection events can occur locally as the results of the generation of small scales along the turbulent cascade. Figure 2 displays the contour map of the proton temperature anisotropy, defined as the ratio between perpendicular and parallel temperature, with respect to the direction of the local magnetic field. The black/white lines indicate the isosurface of the magnetic potential of the inplane magnetic field. It is clearly shown that, in the region of high magnetic stress, the particle velocity distributions depart from the typical configuration of thermodynamical equilibrium showing the generation of temperature anisotropy, both along and across the local magnetic field.

At present, an updated version of the hybrid Vlasov-Maxwell code has been implemented to take into account also the kinetic dynamics of alpha particles (Perrone et al. 2011) with the purpose of providing a more realistic description of the solar wind. In fact the interplanetary medium is constituted predominantly of protons, but a small amount of doubled ionized helium is also present. In recent works, through the statistical analysis of the solar wind data from the Helios spacecraft (Bourouaine et al. 2010, 2011a, 2011b), it has been pointed out that the dynamics of alpha particles can present important signatures of kinetic effects, like temperature anisotropy and heating, that in many situations are more evident than in the

**Fig. 2** Contour plot of the proton temperature anisotropy  $T_{\perp}/T_{\parallel}$ . The *black/white lines* indicate the isosurface of the magnetic potential of the inplane magnetic field; the different colors of the contour lines indicate the different direction of rotation of the vortices (Servidio et al. 2012)



case of protons. In 2011 the updated version of the hybrid Vlasov-Maxwell code (protons and alphas) has been used in 1D-3V phase space configuration (Perrone et al. 2011) to generalize the study of the role of kinetic effects in the longitudinal component of the solar-wind turbulent spectra, including the kinetic dynamics of the alpha particles.

#### 4 Finite Larmor Radius Effects and Nonclassical Transport in Turbulence

There are essentially two approaches to capturing the effects of finite Larmor radius on particle transport in turbulent plasmas, whose relevance to a given physical situation depends on the type of turbulence considered. If the underlying magnetic field is not laminar, in the sense that the field lines deviate from each other or are braided together, it is essential to capture these features in statistical terms, and combine them (Duffy et al. 1995; Hornsby et al. 2010) with a model for particle orbits. For example, guiding centre drift combined with finite Larmor radius excursion may transfer particles between locally neighboring field lines which ultimately diverge substantially. Conversely large Larmor radius excursions may average out the effects of small scale (sub Larmor radius) variations in magnetic field.

If the underlying magnetic field can be considered locally laminar, the gradients of pressure and temperature within the plasma typically act as sources of free energy that can excite electrostatic turbulence. This is usually the dominant source of particle and energy transport in laboratory plasmas, and is expected to arise, beside electromagnetic turbulence, in space and astrophysical plasmas wherever gradients are steep; in foreshock regions, for example Kirk and Dendy (2001), Schmitz et al. (2002a, 2002b); Lee et al. (2005a, 2005b). The effects of the resultant electrostatic turbulence on particle transport, given finite Larmor radius, can be captured in two ways. First, one can implant test particles in a simulation, whose orbits respond to the ambient turbulent fields, but do not generate or act upon them. The ensemble statistics are then calculated. This is particularly appropriate to situations where the electrostatic turbulence can be modeled in quasi-fluid terms. For example, in Hasegawa-Mima turbulence, the effect of finite Larmor radius on the transport of ions, whose guiding centres drift with the  $\mathbf{E} \times \mathbf{B}$  velocity, was first examined in Manfredi and Dendy (1996, 1997). These studies contribute to the understanding of the differential transport of fusion-born alpha particles (3.5 MeV initial energy; large Larmor radius) compared to thermal ions (10 keV; small Larmor radius) in magnetically confined plasmas. The approach to finite Larmor radius adopted in Manfredi and Dendy (1997) is equivalent to multiplying the  $k$ th

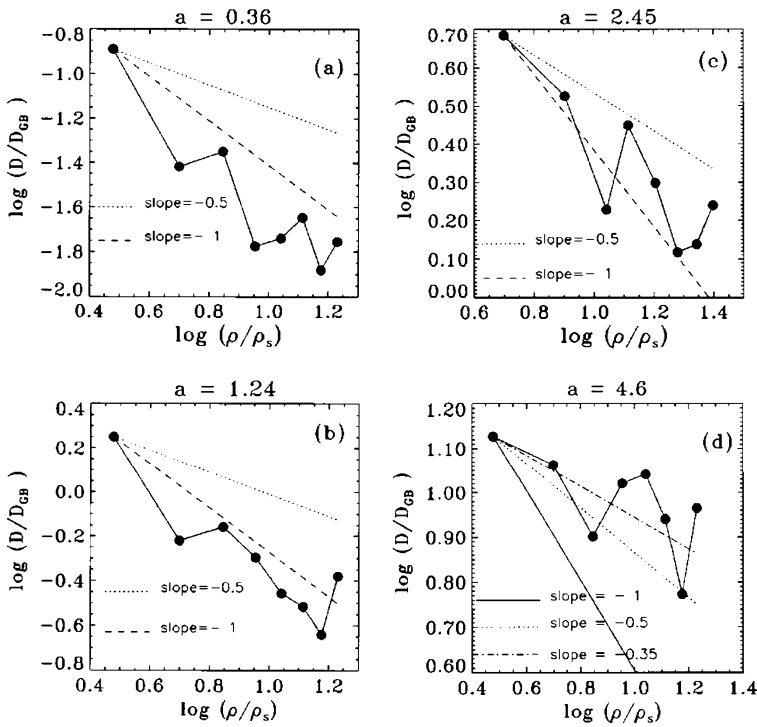


**Fig. 3** Scaling of the diffusion coefficient against Larmor radius on a logarithmic scale (base 10) for four values of the normalized amplitude: (a)  $a = 0.36$ ; (b)  $a = 1.24$ ; (c)  $a = 2.45$ ; and (d)  $a = 4.6$ . The slope  $-0.5$  line (dotted line) corresponds to the large amplitude scaling, while the slope  $-1$  line (broken line) corresponds to small amplitude scaling. In (d) the slope  $-0.35$  is also indicated, which corresponds to a theoretical result for large amplitude. The different regimes of small and large amplitude are clearly visible. Reprinted with permission from Manfredi and Dendy (1997). Copyright (1997), American Institute of Physics

Fourier component,  $E(k)$ , of the electrostatic field, by an effective amplitude  $J_0(k\rho)$ , where  $\rho$  is the Larmor radius and  $J_0$  is a Bessel function (Gustafson et al. 2008). The transport depends also on the normalized strength  $a$  of the field, which scales as the ratio of its root-mean-square amplitude and frequency; see Eq. (8) of Manfredi and Dendy (1997). Figure 3 (Fig. 14 of Manfredi and Dendy (1997)) shows the scaling of ion transport with Larmor radius in Hasegawa-Mima turbulence at different amplitudes.

Subsequent investigations (Annibaldi et al. 2000, 2002) draw attention to the non-Gaussian, strange kinetics statistical properties of the associated transport processes, arising from the interplay between finite Larmor radius ion orbits with coherent nonlinear structures in the turbulence. For example, Fig. 4 (corresponding to Figs. 13 to 15 of Annibaldi et al. (2002)) provides clear evidence of subdiffusion, superdiffusion, and ballistic motion, in addition to normal diffusion, depending on the character of the Hasegawa-Mima turbulence quantified by the plasma  $\beta$  and the magnitude of the Larmor radius. More sophisticated models for electrostatic turbulence have subsequently been studied from the same perspective: for example, the Hasegawa-Wakatani model, in which electrostatic potential and density are treated as independent coupled variables, has recently been extended to incorporate a gradient in the background magnetic field. The associated  $\mathbf{E} \times \mathbf{B}$  transport of test particles is studied in Dewhurst et al. (2009), and finite Larmor radius is incorporated in Gustafson

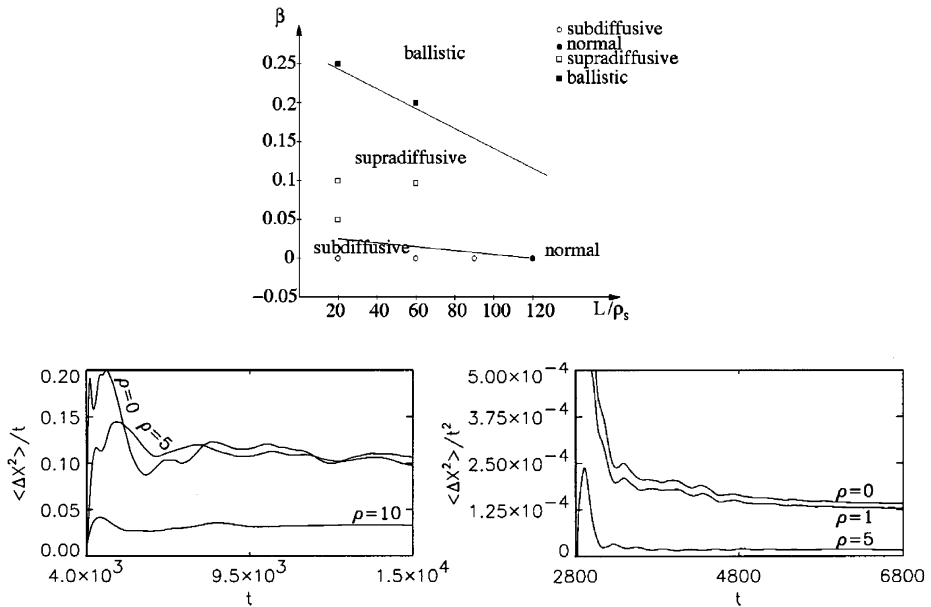


**Fig. 4** *Top:* Dependence of ion transport regimes on plasma inhomogeneity parameter  $\beta$  and the ratio of system size  $L$  to Larmor radius  $\rho$ . *Bottom: (Left)* Dependence of transport on Larmor radius for  $\beta = 0$  and  $L = 120$ , for  $\rho = 0, 5$ , and  $10$ . Mean squared displacement divided by time reveals normal transport with diffusion coefficient decreasing with  $\rho$ . *(Right)* Dependence of transport on Larmor radius for  $\beta = 0.2$  and  $L = 60$ , for  $\rho = 0, 1$ , and  $5$ . Mean squared displacement divided by squared time reveals ballistic transport with coefficient decreasing with  $\rho$ . Reprinted with permission from Annibaldi et al. (2002). Copyright (2002), American Institute of Physics

et al. (2008) and Dewhurst et al. (2010). The latter includes combinations of small-scale turbulence with large scale coherent nonlinear structures, addressed below in Sect. 5. A key physics point emerging from these studies is the centrality of the Weiss field  $Q$ , which is proportional to the difference between squared stress and squared vorticity in the turbulence, in governing the interaction between finite Larmor radius particles and coherent nonlinear structures. This applies both to the spatial distribution of local concentrations of  $Q$  (positive or negative), see for example Figs. 1 and 3 of Annibaldi et al. (2002) and Fig. 2 of Dewhurst et al. (2010), and to the statistics of fluctuations in  $Q$ .

#### 4.1 Test Particle Simulations of Transport in the Presence of Magnetic Turbulence

The transport of plasma particles in the presence of magnetic turbulence can be studied by test particle numerical simulations. Making reference to the solar wind, the background magnetic field is assumed to be constant (although plasma transport in nonhomogeneous systems like the magnetosphere is also relevant (see, e.g., Zimbardo et al. 2010)), while the turbulence properties are varied. In most numerical models, turbulence is represented by a discrete number of modes, with different models having different degrees of anisotropy, dimensionality (1D, 2D, or 3D), and spectral shape. In particular, turbulence anisotropy is described either by the so-called slab turbulence, in which the turbulence wave vectors are parallel to the background field  $\mathbf{B}_0$ , or by the so-called 2D turbulence, in which the turbulence wave vectors are distributed only in the plane perpendicular to  $\mathbf{B}_0$ . Other turbulence models, even nonaxisymmetric, have been developed.

Anomalous transport corresponding to perpendicular subdiffusion was reported by Qin et al. (2002a) in the case of slab turbulence, while parallel diffusion was found to be normal. The perpendicular subdiffusion is a result of particles tracing back the field lines after pitch angle diffusion, and is related to the so-called compound diffusion (Kóta and Jokipii 2000; Webb et al. 2006) discussed in Sect. 2.4. The latter is dependent on the rate of exponential separation of close field lines (e.g., Rechester and Rosenbluth 1978), which is smaller for slab anisotropy and is larger for quasi 2D anisotropy (Zimbaro et al. 2009; Bitane et al. 2010). If the exponential separation of field lines is fast enough, particles which have been pitch angle back scattered will not trace back the original field line, and normal diffusion results. This also means that the antipersistent correlations implied by compound diffusion are destroyed by the stochasticity of field lines. Indeed, for a composite model of slab plus 2D turbulence with 80 % of fluctuation energy in the 2D spectrum, Qin et al. (2002b) have recovered diffusion also perpendicular to  $\mathbf{B}_0$ , in agreement with the fact that the exponentiation of field lines is faster for 2D turbulence.

The influence of turbulence anisotropy on the structure of magnetic flux tubes has been studied by Zimbaro et al. (2004) with a fully 3D spectrum where quasi-slab turbulence is represented by a cigar-shaped distribution of wave vectors along  $\mathbf{B}_0$ , while the quasi-2D turbulence is represented by a pancake-shaped distribution of wave vectors in the plane perpendicular to  $\mathbf{B}_0$ . The axes of the constant amplitude ellipsoids in phase space are given by the inverse of the correlation lengths  $l_{\parallel}$  and  $l_{\perp}$  (Zimbaro et al. 2000a), with  $l_{\parallel}/l_{\perp} \gg 1$  ( $\ll 1$ ) corresponding to the quasi-2D (quasi-slab) anisotropy. Zimbaro et al. (2004) have shown that indeed the complexity of the magnetic flux tubes grows with  $l_{\parallel}/l_{\perp}$  and with the Kubo number, see Fig. 5.

Zimbaro (2005) and Zimbaro et al. (2006) studied the effect of turbulence anisotropy on particle transport with the above 3D anisotropic numerical model. Here and in next sections, the anomalous transport exponent is indicated by  $\gamma \equiv 2H$ , where  $H$  is the Hurst exponent. It is found that for quasi-slab turbulence, transport is anomalous, corresponding to parallel superdiffusion with  $\gamma \simeq 1.2$ , and to perpendicular subdiffusion with  $\gamma \simeq 0.8$ . The flatness of the distribution of field line positions is much larger than the Gaussian value of 3, confirming that anomalous diffusion is related to non-Gaussian statistics and heavy tailed distributions. On the other hand, going to the isotropic case, parallel transport is superdiffusive with  $\gamma \simeq 1.4$ , while perpendicular transport is normal. In the quasi-2D case, both parallel and perpendicular transport are found to be normal, confirming the results of Qin et al. (2002b). These results emphasize the importance of turbulence anisotropy. Parallel superdiffusion with  $\gamma \simeq 1.3$  and perpendicular subdiffusion with  $\gamma \simeq 0.75$  were also found by Shalchi and Kourakis (2007) by injecting test particles in a composite turbulence model with 20 % slab turbulence and 80 % 2D turbulence, thus expanding the range of cases when superdiffusion can be found. On the other hand, the transport regime also depends on the particle energy, in particular through the ratio between the particle Larmor radius  $\rho$  in the background magnetic field and the turbulence correlation lengths. Pommois et al. (2007) find that for  $\rho/l_{\perp} = 0.001\text{--}0.01$ , parallel superdiffusion and perpendicular subdiffusion can be found, while normal diffusion is obtained for  $\rho/l_{\perp} \sim 0.1$  (see Fig. 6). These results correspond to the fact that the turbulence energy density scales as  $E(k) \sim k^{-5/3}$ , so that higher energy particles, having larger Larmor radii, resonate with longer wavelength fluctuations which have larger amplitude; correspondingly, pitch angle scattering is faster, and the long parallel displacements which give rise to superdiffusion are no longer found. Therefore normal diffusion results. Interestingly, from Fig. 6 one can see that for  $\rho/l_{\perp} \sim 1$  parallel superdiffusion is obtained again: this is because in the turbulence model considered by Pommois et al. (2007) most of the fluctuation energy is at scales smaller than  $l_{\perp}$ . In such a case, most fluctuations are average out by the large Larmor radius, and pitch angle scattering is reduced.

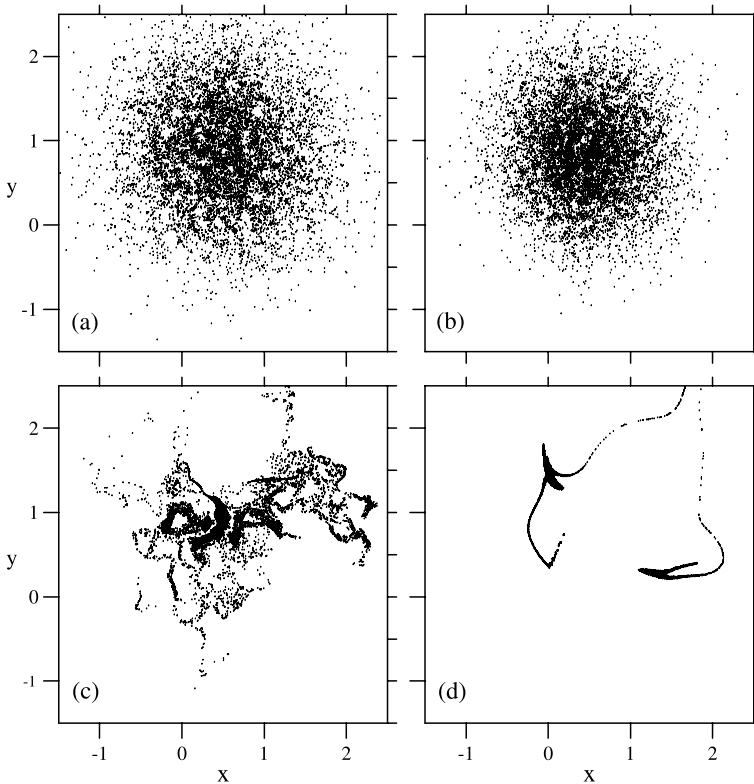


**Fig. 5** Cross section of the magnetic flux tube structure of an initially circular flux tube, for different degrees of turbulence anisotropy: **(a)** quasi-2D anisotropy; **(b)** isotropic turbulence; **(c)** and **(d)** quasi-slab anisotropy, for two different ratios  $l_{\parallel}/l_{\perp}$ . Reprinted with permission from Zimbaro et al. (2004). Copyright 2004 by the American Geophysical Union

Recently, Tautz and Shalchi (2010) have found that perpendicular transport is clearly subdiffusive, with  $\gamma \simeq 0.6$ , in the case of slab turbulence. Normal perpendicular diffusion is almost recovered in the case of isotropic or two-component (slab + 2D) turbulence, but a weakly subdiffusive behavior remains, corresponding to  $\gamma = 0.83\text{--}0.94$ . According to Tautz and Shalchi (2010), perpendicular subdiffusion is the rule rather than the exception. An interesting recent study shows that perpendicular subdiffusion is obtained for magnetostatic slab turbulence, while the inclusion of wave time dependent electric and magnetic field leads to parallel superdiffusion as well as to particle energization (Tautz 2010; Gustafson et al. 2012a). Such an energization is due to stochastic (second order) Fermi acceleration. A similar process has also been investigated by Perri et al. (2007) and by Perri et al. (2011) in two-dimensional and three-dimensional numerical models where test particles interact with time dependent electromagnetic fluctuations. The stochastic interaction leads to superdiffusion in real space, diffusion in momentum space, and to a particle energization characterized by both energy gains and energy losses, which are typical of a second-order Fermi process. The consequences of occasional collisions for particle transport in magnetic turbulence were quantified using a computational Vlasov-Fokker-Planck model by Hornsby et al. (2010). This enables one to identify the connection to classic transport paradigms important for laboratory plasmas, such as quasi-linear and gyro-Bohm, and the extent to which

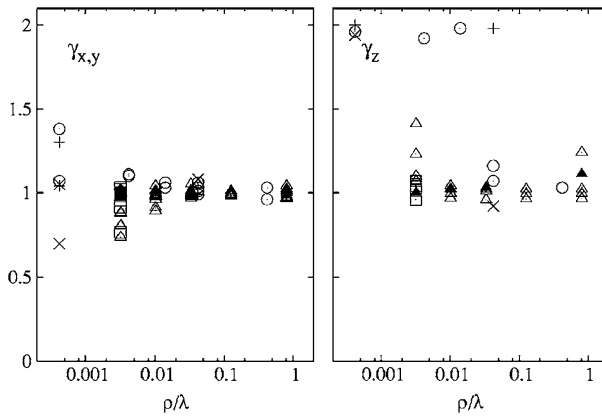


**Fig. 6** Anomalous diffusion exponent  $\gamma$  versus the ratio of Larmor radius  $\rho$  over turbulence correlation length  $\lambda$ . *Left panel:* exponents  $\gamma_x$  and  $\gamma_y$  for transport in the plane perpendicular to the average magnetic field. *Right panel:* exponent  $\gamma_z$  for transport parallel to the average magnetic field. The different symbols denote different turbulence levels: *plus signs*,  $\delta B/B_0 = 0.05$ ; *circles*,  $\delta B/B_0 = 0.1$ ; *crosses*,  $\delta B/B_0 = 0.2$ ; *triangles*,  $\delta B/B_0 = 0.5$ ; *squares*,  $\delta B/B_0 = 1.0$ . Reprinted with permission from Pommois et al. (2007). Copyright (2007), American Institute of Physics

these provide a reliable guide depending on the strength of the turbulence. All these results agree with the main trend of the above quoted works, and we note that the various studies use substantially different numerical realizations of turbulence, so that the cases when anomalous transport is obtained emerge as being independent of the numerical scheme.

#### 4.2 Vlasov Simulations

Let us now turn to cases where the turbulence is fundamentally kinetic in nature, so that the self-consistent evolution of particle dynamics, including finite Larmor radius, together with fields is central to the model. It is still possible to adopt a test particle approach in such cases, and to compute ensemble transport properties. This applies to Vlasov and particle-in-cell (PIC) kinetic simulations of turbulence. For example, Fig. 16 of Manfredi et al. (1996) shows diffusion coefficients inferred in this way from finite ion Larmor radius Vlasov gyrokinetic simulations of ion temperature gradient-driven turbulence. A systematic analysis of fields experienced by finite Larmor radius ions undergoing acceleration in PIC simulations of turbulence at solar system and astrophysical shocks is given in Lee et al. (2005a, 2005b).

The role of kinetic effects in turbulent plasmas has become a subject of increasing interest within space plasma physics. The interstellar medium is generally observed from spacecraft measurements (Bruno and Carbone 2005; Marsch 2006) to be in a fully turbulent regime. Along the turbulent cascade, nonlinear local couplings transfer energy from low to high frequencies. At low MHD frequencies, the energy spectra of the magnetic fluctuations display a slope in agreement with the Kolmogorov 5/3 law for fluid turbulence. When the energy is transferred towards increasingly high frequencies (increasingly small scales), kinetic effects come into play, leading to significant changes in the spectral properties (Alexandrova et al. 2009; Sahraoui et al. 2010). The first evident modification has been identified at length scales of the order of typical ion kinetic scales, namely the inertial length and Larmor radius (Bale et al. 2005). For values of the plasma parameter  $\beta_p$  (ratio between kinetic and magnetic pressures) of order unity, typical of the solar wind plasma away from the Sun, the inertial length and Larmor radius are comparable in size. Linked to these spectral changes,

the signatures of finite Larmor radius effects have been also recovered from the analysis of particle velocity distributions. Significant distortions and non-Maxwellian features have been observed both for the proton and the alpha particle velocity distributions. For example, in recent work by Bourouaine et al. (2010, 2011a, 2011b) the generation of temperature anisotropy has been analyzed for the solar wind particle velocity distributions from the Helios spacecraft. It is found that more significant effects are visible for alpha particles than for protons (Chen et al. 2011). In this case the cyclotron resonance predicts that alpha particles stay in resonance with the waves having a lower frequency than those that the protons resonate with, and thus they can receive by absorption more wave energy for the turbulent spectrum than protons (Miller 1998).

The hybrid Vlasov-Maxwell code, briefly described in Sect. 3, has been employed in 2D-3V phase space configuration to identify the role of kinetic effects in the range of spatial scales close to the proton Larmor radius, in a plasma composed of kinetic ions (protons and alpha particles) and fluid electrons in conditions typical of the solar-wind environment. Here we discuss the numerical results for the kinetic dynamics of alpha particles and protons in decaying turbulence. The plasma dynamics is investigated in a doubly periodic  $x-y$  spatial domain perpendicular to a background magnetic field (Perrone et al. 2013). In the initial equilibrium the ion species have homogeneous densities and Maxwellian velocity distributions. The equilibrium configuration is perturbed by a 2D spectrum of fluctuations for the magnetic and proton velocity fields. Energy is injected with random phases and wave numbers in the range  $0.1 < k\rho_p < 0.3$ , where  $k = 2\pi m/L$ , with  $2 \leq m \leq 6$ . The rms of the initial magnetic perturbations is  $\delta B/B_0 \simeq 0.3$ . Neither density disturbances nor parallel variances are imposed at  $t = 0$ . The proton plasma beta is  $\beta_p = 2v_{th,p}^2/V_A^2 = 2$  and the electron to proton temperature ratio is  $T_e/T_p = 1$ . For the alpha particles we set  $Z_\alpha = 2$ ;  $m_\alpha/m_p = 4$ ,  $n_{0,\alpha}/n_{0,p} = 5\%$  and  $T_\alpha/T_p = 1$ . With this choice, the alpha particle thermal speed is  $v_{th,\alpha} = v_{th,p}/2$ .

The statistical analysis is performed at a given instant of time at which the level of the turbulent activity has attained its maximum value. During the evolution of turbulence, coherent structures and strongly sheared flows appear in the 2D pattern in physical space. In Fig. 7 [panel (a)], the shaded contours of the out-of-plane total current density  $j_z$  are represented together with the contour lines of the magnetic potential  $A_z$  of the inplane magnetic field. Different directions of rotation of the vortices in the contour lines of  $A_z$  are indicated by different colors (black and white). This figure shows that the current density becomes very intense in between the magnetic islands, and reconnection events occur at the X-points of  $A_z$ , indicated in the figure by red crosses.

In order to quantify the kinetic effects on alpha particles and protons, generated when the energy is transferred towards short scales along the turbulent cascade, the temperature anisotropy for each ion species has been computed as the ratio between perpendicular and parallel temperatures with respect to the local magnetic field:  $A_i = T_\perp^{(i)}/T_\parallel^{(i)}$ , where  $i$  stands for protons and alpha particles, respectively. The temperature of each ion species can be evaluated as the second order velocity moment of the particle distribution function, through a direct integration in velocity space:

$$T_i = \frac{m_i}{3n_i} \int (\mathbf{v} - \mathbf{u}_i)^2 f_i d^3v \quad (i = p, \alpha) \tag{18}$$

where  $f_i$  is the ion distribution function,  $n_i = \int f_i d^3v$  is the particle density and  $\mathbf{u}_i = \int \mathbf{v} f_i d^3v / n_i$  is the ion-bulk velocity. Even though the initial conditions of the simulations are set up so as to have isotropic temperatures for both protons and alpha particles at  $t = 0$

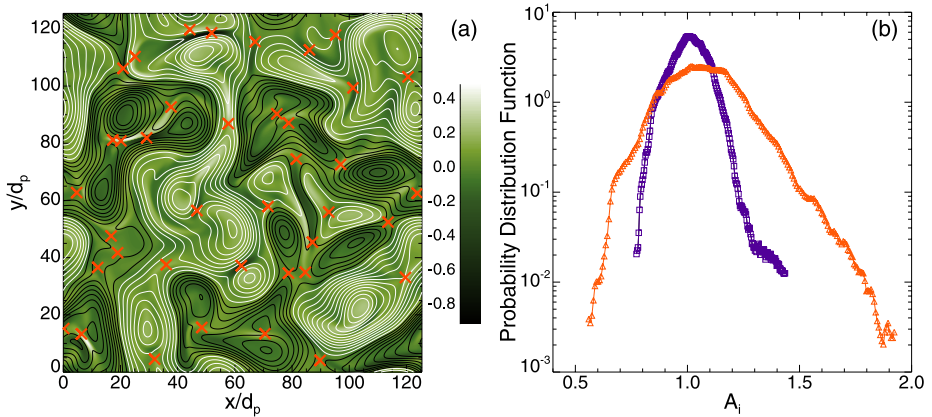


**Fig. 7** Panel (a): Contour plot of the out-of-plane total current density ( $j_z$ ). The isolines of the magnetic potential  $A_z$  are indicated by black/white lines. The positions of the X-points, where reconnection occurs, are indicated by thick red crosses. Panel (b): PDF of the temperature anisotropy  $A_i$  of protons (blue-square line) and alpha particles (red-triangle line) at the maximum of the turbulent activity ( $t = 40$ )

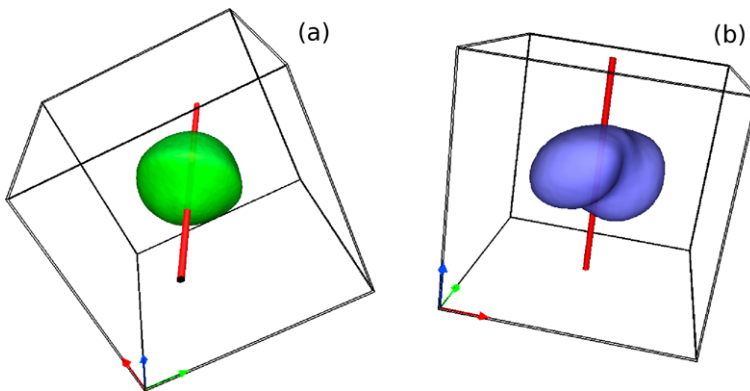


**Fig. 8** Isosurfaces of the proton (a) and alpha particle (b) velocity distributions at two different spatial locations, where  $A_p, A_\alpha > 1$ . The direction of the local magnetic field is displayed as a red tube

( $A_i = 1$ ), it is found that, during the system evolution, the anisotropy index  $A_i$  can depart significantly from unity for both ion species. To quantify this statement, the probability distribution function (PDF) of  $A_i$  has been evaluated at the time when the simulated turbulence is strongest. The results are shown in Fig. 7 [panel (b)] for protons (blue-square line) and alpha particles (red-triangle line). Both ion species develop temperature anisotropy with respect to the directions parallel and perpendicular to the local magnetic field. This anisotropy is significantly more evident for alpha particles than for protons, and this corresponds with recent solar-wind observations from the Helios spacecraft (Bourouaine et al. 2010, 2011a, 2011b).

The isosurfaces of the particle velocity distribution, evaluated at the spatial locations where the anisotropy index reaches its maximum value, are plotted in Fig. 8 for protons [panel (a)] and alpha particles [panel (b)]. In each panel, the direction of the local magnetic field is displayed as a red tube. From this figure, it is evident that, while the proton velocity distribution remains quite close to the Maxwellian spherical shape, the alpha-particles

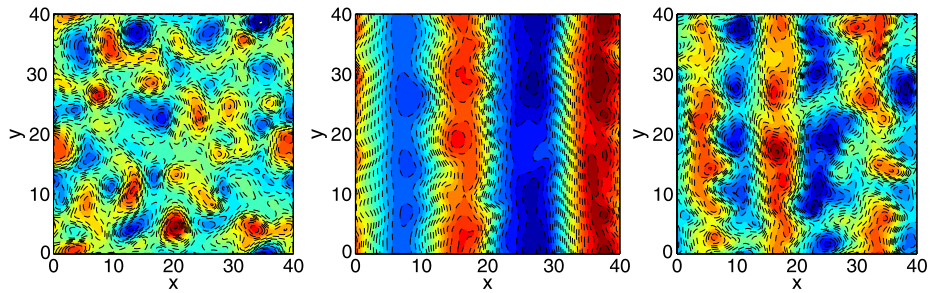


**Fig. 9** Electrostatic potential in the plane perpendicular to the magnetic field obtained from a generalized Hasegawa-Wakatani model in three regimes: (*Left*) Small scale turbulence with damped zonal flows; (*Centre*) Self-generated zonal flows dominate; (*Right*) Energy of zonal flows and of small scale turbulence constrained to be equal. Reprinted with permission from Dewhurst et al. (2010). Copyright (2010), Institute of Physics

velocity distribution is evidently shaped by kinetic effects, displaying a certain elongation with the formation of a bubble structure in the direction perpendicular to the local magnetic field. These typical non-Maxwellian velocity distributions are common features of solar-wind plasmas (Marsch et al. 1982a, 1982b; Bourouaine et al. 2010, 2011a, 2011b).

The numerical results described here suggest that Eulerian Vlasov simulations can provide a noiseless multi-ion description of collisionless plasmas in physical conditions close to reality and represent an indispensable tool for the interpretation of the complex phenomenology recovered in the solar-wind observations.

## 5 Non-diffusive Transport Arising from the Combination of Small Scale Turbulence with Large Scale Coherent Nonlinear Structures

In well diagnosed laboratory plasmas, coexistence and interaction (Fujisawa 2011; Diamond et al. 2011) between small scale drift turbulence (Tynan et al. 2009) and large scale coherent nonlinear structures—zonal flows (Diamond et al. 2005), streamers (Yamada et al. 2008), and other objects that exhibit long range correlation (Inagaki et al. 2011)—is an established feature which is central to the phenomenology of the global system (Wagner 2007). Approaches to modelling this span the zero-dimensional Lotka-Volterra predator-prey paradigm (Malkov and Diamond 2009), nonlinear few-wave coupling (Manfredi et al. 2001), and large scale numerical simulations, which however are challenged by the need to incorporate a wide range of physically relevant lengthscales.

It is therefore interesting to include finite Larmor radius test particle dynamics in a plasma model which can incorporate the coexistence and interaction of small scale turbulence and coherent nonlinear structures. Figure 9 shows three regimes of electrostatic turbulence in the generalized Hasegawa-Wakatani model of Dewhurst et al. (2009), with small scale turbulence coexisting with zonal flows in the right-hand panel. The corresponding transport properties of ensembles of test particles that have finite Larmor radius  $\rho$  of different sizes, obtained in Dewhurst et al. (2010), are shown in Figs. 10 and 11. In Fig. 10, for convenience we quantify the mean squared spatial dispersion in terms of a diffusion coefficient, however Fig. 11 emphasizes that the transport is not necessarily diffusive. Furthermore, where it is diffusive, the rate of transport is substantially different between the cases where small scale turbulence is dominant and where it coexists with zonal flows. It is evident that the transport properties are sensitive, in particular, to the size of Larmor radius  $\rho$

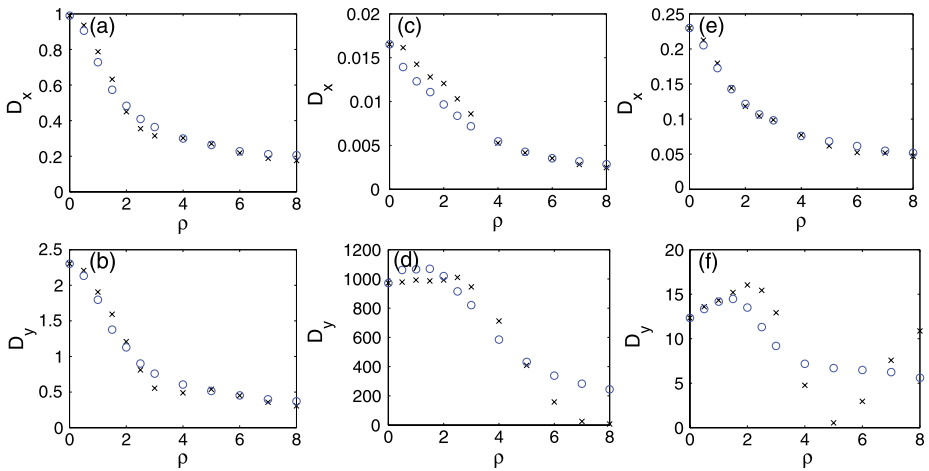


**Fig. 10** Test particle diffusion coefficients, as functions of Larmor radius  $\rho$ , in the different turbulence regimes of Fig. 9. Directions of axes are perpendicular ( $x$ ) and parallel ( $y$ ) to the dominant orientation of zonal flows, where they exist. *Crosses* indicate results when all the test particles share the same Larmor radius  $\rho$ ; *circles* indicate results when the Larmor radii are distributed around a most probable value  $\rho$ . Reprinted with permission from Dewhurst et al. (2010). Copyright (2010), Institute of Physics

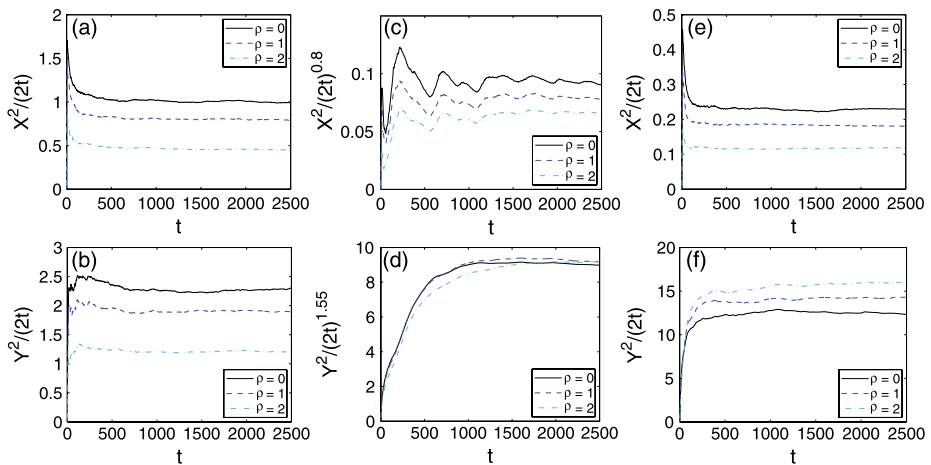


**Fig. 11** Test particle dispersion in the  $x$  (top) and  $y$  (bottom) directions, as functions of time, for three different values of Larmor radius  $\rho$ . The three vertical pairings correspond to the three turbulence regimes of Fig. 9. (Left) normal diffusion; (Centre) subdiffusion in  $x$  and superdiffusion in  $y$ ; (Right) normal diffusion at rates substantially lower in  $x$  and higher in  $y$  than in the (Left) case. Reprinted with permission from Dewhurst et al. (2010). Copyright (2010), Institute of Physics

relative to typical scale of the small scale turbulent vortices ( $\rho = 3$ ) and the half-wavelength between zonal flows ( $\rho = 8$ ) (Hauff and Jenko 2008).

Another useful test-bed is found in the injection of suprathermal ions into turbulence produced in a simple magnetized torus (SMT). Here, in Fig. 12, we present three simulated, representative examples of transport for an injected beam of mono-energetic ions (Gustafson and Ricci 2012): subdiffusion at  $\mathcal{E} = 250$ , diffusion at  $\mathcal{E} = 25$ , and superdiffusion at  $\mathcal{E} = 5$ ,

**Fig. 12** Radial positional dispersion  $\sigma^2$  for turbulent suprathermal ion transport for three different injection energies [ $\mathcal{E} = 5$  (red, topmost curve),  $\mathcal{E} = 25$  (black, middle curve) and  $\mathcal{E} = 250$  (blue, lower curve)] showing representative examples of superdiffusion, diffusion, and subdiffusion, respectively. We express  $\sigma$  in terms of  $\rho_s$ , the ion sound radius for the SMT plasma, and  $t$  in terms of  $\Omega$ , the suprathermal ion Larmor frequency. Reprinted with permission from Gustafson and Ricci (2012). Copyright (2012), American Institute of Physics

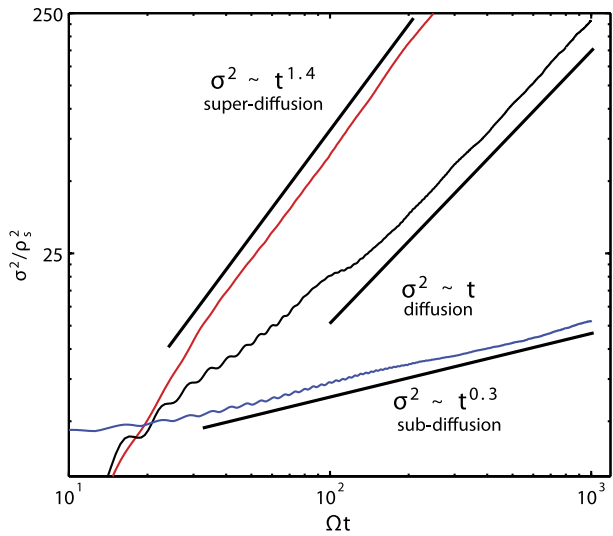


**Table 1** Measured power law exponent for  $\sigma^2(t)$ ,  $p(\Delta r)$  and  $\Delta r(\Delta t)$

$\gamma \pm 0.1$	$\mu \pm 0.1$	$\nu \pm 0.1$
1.4	3.0	0.7
1.0	3.5	0.9
0.3	3.5	0.15

where  $\mathcal{E} \equiv m v_0^2 / (2 T_e)$  is the initial ion energy normalized to the plasma electron temperature,  $T_e$ . For these cases, the turbulence amplitude in the SMT is such that  $\xi = 0.8$ , where  $\xi \equiv e \delta \phi / T_e$  and  $\delta \phi$  is the standard deviation of the amplitude of the electrostatic potential. In Fig. 12, the mean square deviation of particle radial positions,  $\sigma^2 \sim t^\gamma$ , is shown as a function of time. The value of  $\gamma$  is determined by best-fitting the growth of  $\sigma^2$  with a power-law curve during the turbulence interaction regime (described below). The values of  $\gamma$  for the three different cases are summarized in Table 1. Error in the fitted values is of order  $\pm 0.1$ . The significant differences in the values of  $\gamma$  for different energies result from the interplay of turbulent diffusion, gyroaveraging, and geometrical effects. Essentially, the spreading is superdiffusive when both gyroaveraging and vertical  $\nabla \mathbf{B}$  drifts are small, while the spreading becomes subdiffusive,  $\gamma \rightarrow 0$ , when vertical drift averaging becomes dominant over turbulent diffusion, as described in more detail in Gustafson et al. (2012b). Note that periodic oscillations in  $\sigma^2(t) \equiv \langle \Delta r^2(t) \rangle$  are caused by the ion gyromotion.

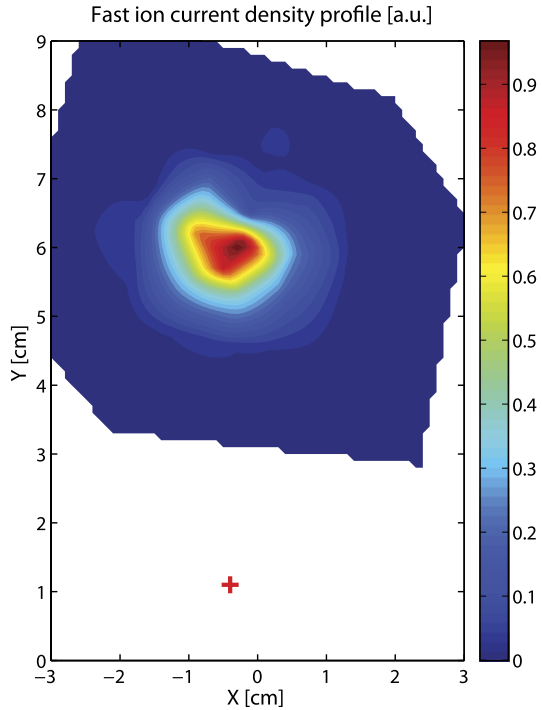
The SMT study thus establishes that suprathermal ion spreading can be subdiffusive, diffusive, or superdiffusive depending on the ion energy and turbulence amplitude. In previous works, superdiffusion and subdiffusion have been used to model transport in plasmas, see e.g. Rechester and Rosenbluth (1978), del Castillo-Negrete (1998), Pommois et al. (2001), Ruffolo et al. (2003), Hauff et al. (2007), Sanchez et al. (2008), Burillo et al. (2009). The coexistence of the three regimes was also observed in Abdullaev (2000). The SMT simulations show that the diffusion approximation is valid only locally, or, stated otherwise, the effective local suprathermal ion diffusivities can show strong time dependence. For example, they can be significantly different from thermal ion diffusivities computed for similar turbulent plasmas in Ricci and Rogers (2009).

The assumption of coupled step sizes,  $\Delta r$ , and step durations,  $\Delta t$  in the CTRW framework, see Sect. 2.3, determines  $\gamma$  as a function of the two parameters  $\nu$  and  $\mu = \alpha + 1$  (Klafter et al. 1987). In particular  $\mu$  can be found from the step-size PDF,  $p(\Delta r) = \int \phi d\Delta t$ , and  $\nu$  is inferred from the relation between  $\Delta t$  and  $\Delta r$ . The SMT results from TORPEX simulations give superdiffusive and diffusive values of  $\nu$  half the magnitude of those found by Zimbaro et al. (2000b). This is sensible, since that study of magnetic turbulence used a constant, unidirectional accelerating electric field, leading to larger  $\Delta r$  for a given  $\Delta t$ . The analytical predictions of the dependence of  $\gamma$  on  $\nu$  and  $\mu$  presented in Klafter et al. (1987) succeed in predicting the character of the SMT transport with gratifying accuracy (see Table 1). For example, the subdiffusive  $\gamma$  is predicted by Klafter et al. (1987) to be  $\gamma = \nu\mu' - 1 \simeq 0.4$  with  $\mu' = \mu - 1 + 1/\nu$ , in close agreement with the observed  $\gamma = 0.3$ . Similarly, all three examples of suprathreshold ion transport match predictions of the Klafter walk theory (Gustafson and Ricci 2012).

Having reviewed the theory and modeling of suprathreshold ion transport in turbulent plasmas for the SMT configuration, we discuss here how it can be extended to the interpretation of TORPEX experimental data and show an exploratory comparison between experiments and simulations. TORPEX is an SMT (1 m major radius, 0.2 m minor radius) characterized by low plasma densities ( $n_e \approx 10^{16}$ – $10^{17}$  m $^{-3}$ ) and temperatures ( $T_e \sim 5$ – $20$  eV). TORPEX is equipped with an extensive set of diagnostics allowing high-resolution measurements of plasma parameters and wave fields throughout the plasma cross-section. Plasmas of different gases can be produced and sustained by microwaves in the electron cyclotron frequency range,  $f = 2.45$  GHz. A number of turbulence regimes have been characterized experimentally and validated numerically (Ricci and Rogers 2010; Ricci et al. 2009, 2011) for TORPEX. Here, a scenario with  $B_t = 74$  mT and  $B_v = 2$  mT is used, resulting in a SMT with vertical magnetic field line return distance  $\Delta D \approx 17$  cm, which is dominated by an ideal interchange mode with wavenumbers  $k_{\parallel} \approx 0$ , and,  $k_{\perp} \approx 37$  m $^{-1}$ . This scenario, similar to those extensively studied in Furno et al. (2008a, 2008b), Müller et al. (2007), Theiler et al. (2008, 2009), Diallo et al. (2008), Podestà et al. (2008), Labit et al. (2011), Furno et al. (2011) using electrostatic probes, is characterized by the presence of a region on the low-field side where coherent structures are observed to propagate radially outward resulting in intermittent non-Gaussian transport of particles, heat, momentum and current.

Suprathreshold Li $^{6+}$  ions are injected using a miniaturized ion source, such that Li $^{6+}$  ion currents up to 10  $\mu$ A can be obtained (Plyushchev et al. 2006). The source is motorized and can be continuously moved over a toroidal distance of 50 cm between each discharge. Ion energy and current density profiles are measured using a miniaturized gridded energy analyzer (GEA), which consists of two identical GEAs facing opposite directions for background noise subtraction. Each detector has small dimensions (15 mm in diameter, 70 mm in length and in inlet diameter of 8 mm), and is able to measure fast ion currents as small as 0.1  $\mu$ A. Synchronous detection is used to increase the signal-to-noise ratio by modulating the emitter bias voltage at a given frequency ( $\sim 1$  kHz). The GEA detector is installed on a two-dimensional moving system, which enables reconstruction of the ion current density profile with a spatial precision of 5 mm over almost the entire poloidal cross section at each toroidal position. In the series of experiments described here, Li $^{6+}$  ions with energy of  $\sim 70$  eV  $\gg T_e$  are injected horizontally in the coherent structure region. The time average electron density at the injection location is  $\approx 5 \times 10^{15}$  m $^{-3}$  and the standard deviation of the floating potential time series, indicating the level of fluctuations, is  $\approx 1$  V. Figure 13 shows an example of a fast ion current density profile at a toroidal distance of  $\approx 54$  cm from the source. The red cross indicates the position of the injection, showing the displacement of the beam spot due to the vertical drift. Measurements are made with and without plasma, in the

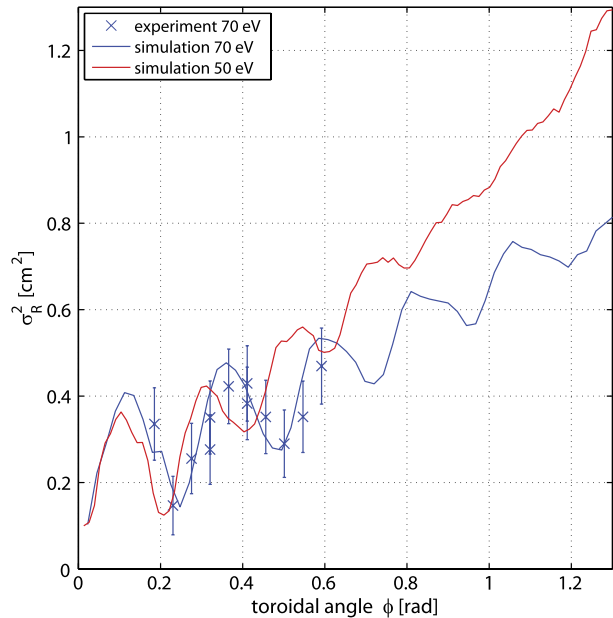
**Fig. 13** Experimental current density profile of fast ions with energy  $E = 70$  eV measured at  $\sim 54$  cm from the fast ion source. The position of the fast ion source is indicated by the *red cross*



presence of magnetic fields. The radial spatial variances of the fast ion current profiles as a function of the toroidal angle are shown in Fig. 14.

To interpret the experimental data, trajectories of tracer  $\text{Li}^{6+}$  ions are integrated in a simulated turbulent electrostatic field driven by the ideal interchange, which is calculated from 2D implementation of the drift reduced Braginskii fluid equations (Gustafson et al. 2012a). Turbulence simulations are performed with different values of the particle and heat sources in order to match experimental profiles. At the injection point, the fluctuation level of the floating potential is higher in the simulation than in the experiment. In order to match the potential fluctuations, the simulated plasma potential fluctuations, are rescaled. Tracer  $\text{Li}^{6+}$  ion trajectories are computed using source parameters based on measurements done without a magnetic field, and 10000 particles are launched with initial parameters modeled with Gaussian distributions. A synthetic diagnostic, mimicking the detector, computes 3D (Bovet et al. 2012; Gustafson et al. 2012a) profiles of the fast-ion current density for comparison with the experimental data. Figure 14 displays the radial variance of the beam profiles along the toroidal direction obtained with the synthetic diagnostic, from the simulations, and from experimental measurements. They show remarkable agreement. The oscillations of the variance of the beam due to the Larmor motion of the particles are clearly evident. The turbulent broadening of the beam is revealed by the radial variance of the beam which increases as a function of the distance from the source. Numerical simulations at later times indicate that, in these conditions, fast ions undergo subdiffusive transport with  $\gamma \approx 0.78$ . The same figure also shows the variance of the beam profiles of simulated data for  $\text{Li}^{6+}$  energy  $\approx 50$  eV, revealing a transition to a superdiffusive regime with  $\gamma \approx 1.2$ . Experimental measurements continue to investigate this new regime.

**Fig. 14** Radial  $\sigma^2$  as a function of the toroidal distance computed with the synthetic diagnostic for  $E = 70$  eV and  $E = 50$  eV from numerical simulations. Experimental data for the case  $E = 70$  eV are also shown revealing good agreement with the simulations



## 5.1 Shock Waves

Shock waves are distinctive large scale nonlinear structures which are observed both in laboratory plasmas and in the solar wind. In space and astrophysical plasmas, shock waves are considered to accelerate particles and cosmic rays, which then propagate both upstream and downstream of the shock. Clearly, such a propagation is influenced by the magnetic turbulence in the medium (Giacalone 2004, 2011). A relevant example where particle transport can be studied *in situ* is that of particles accelerated at shock waves in the solar wind: the energetic particles reach energies of order of 1–10 MeV, and are clearly distinguishable from the background plasma. This gives the possibility to distinguish between diffusive and non-diffusive transport by studying the energetic particle profiles upstream of the shock. Indeed, Perri and Zimbaro (2007, 2008a) have shown that while in the case of normal diffusion the flux of energetic particles upstream of the shock corresponds to an exponential decay, in the case of superdiffusion one has a power law decay. In particular, Perri and Zimbaro (2007, 2008a, 2009a) have shown that electron transport upstream of the shocks associated with corotating interaction regions (CIRs) detected by the Ulysses spacecraft in the solar wind at 4–5 AU is superdiffusive, with  $\gamma \simeq 1.1$ –1.7. Also, ion transport upstream of CIR shocks is found to be normal in most cases, although a slightly superdiffusive case with  $\gamma \simeq 1.1$  is found at a CIR shock detected by Voyager 2 at 6.9 AU. The more decidedly superdiffusive behavior of electrons has been ascribed to the fact that electrons have smaller gyroradii than ions, and therefore the resonant interaction with turbulence happens at larger wavenumbers, where the wave power is less: this favors weak pitch angle scattering and hence superdiffusion (Perri and Zimbaro 2007, 2008a). On the other hand, analyzing the Voyager 2 data for low energy particles, Perri and Zimbaro (2009b) have shown that ion transport upstream of the solar wind termination shock at 84 AU is superdiffusive, too, with  $\gamma \simeq 1.3$ . Perri and Zimbaro (2009b) have interpreted this result as due to the decrease of the magnetic fluctuation amplitude, which causes weaker pitch angle scattering.

Recently Sugiyama and Shiota (2011), using ACE data, have found superdiffusive proton transport with  $\gamma \simeq 1.3$  upstream of a shock at 1 AU driven by a coronal mass ejection. They also find that the level of magnetic fluctuations is not so small for the event considered (in contrast to what can be assumed for the heliopause termination shock at 84 AU), therefore pitch angle scattering should not be so weak. Sugiyama and Shiota (2011) propose that superdiffusion is due to the fact that the wave particle interaction falls into a nonlinear regime, where the quasilinear pitch angle diffusion coefficient no longer applies. In other words, quasilinear theory overestimates the pitch angle diffusion rate. Thus the experimental observation of superdiffusion gives information on the efficiency of wave particle interactions in the nonlinear regime, too, and this compares well with the results of Vlasov simulations reported in Sect. 3.

## 6 Avalanching Transport Conditioned by Critical Gradient Instabilities

The exploitation of thermonuclear fusion plasmas as a mean of producing electricity requires one to confine the thermal energy a hot plasma of temperature  $T \simeq$  a few tens of KeV and density  $n \simeq 10^{20} \text{ m}^{-3}$  for a relatively long time  $\tau \simeq$  a few seconds. As it is well known, this plasma must exceed the Lawson condition  $n \cdot \tau > 3 \cdot 10^{20} \text{ s/m}^3$  to reach ignition. Magnetically confined plasmas, such as those in a tokamak, attempt to reach these conditions by trapping the plasma inside a set of closed, toroidal magnetic surfaces nested around a magnetic axis. Tokamaks and stellarators are realizations of this idea. However, the large radial gradients in pressure, temperature and density that these plasmas must sustain act as free-energy sources for many instabilities. These drive the turbulence which dominated the radial transport inside all these devices. The control of these losses is essential for the success of the fusion program. Traditionally, they have been quantified by using *effective transport coefficients*, obtained from direct measurement or from theoretical models with varying degree of complexity. However, there is much evidence to suggest that radial turbulent transport in these devices can behave in a very non-diffusive manner. This reduces confidence in the extrapolation of these coefficients to parameter regimes outside our current range of operation, which is necessary when designing new and larger devices.

Adoption of the sandpile paradigm (Bak et al. 1988; Dendy and Helander 1997, 1998; Helander et al. 1999; Dendy et al. 2007) in studies of global energy confinement and transport in laboratory and space plasmas is driven by both observational and theoretical considerations. The essence of the sandpile paradigm reflects everyday intuition, as follows. The system is fuelled, for example by the addition of grains at its centre. Local redistribution of sand arises when a critical gradient is exceeded. This may trigger redistribution at neighboring points, and so on progressively, giving rise to avalanching transport events, after which the gradient in affected regions is reset to a value below critical. The probability distribution of the frequency of occurrence of avalanches as a function of their magnitude may be scale-free, for example power-law, implying the existence of correlations on all scales. This portfolio of basic ingredients—energy fuelling, energy storage, and energy release through potentially large scale impulsive events that are conditioned by a critical gradient—maps well to the basic physics of macroscopic plasma systems. For example, a planetary magnetosphere can be viewed as a plasma and energy storage system, driven by the solar wind and subject to impulsive energy release events in the magnetotail and at the dayside magnetopause, which occur when critical gradients associated with the reconnection process are exceeded. Sandpile models have proven successful for magnetospheres (Chapman et al. 1998, 1999; Watkins et al. 1999, 2001) and for accretion disks (Dendy et al. 1998), as has a similar approach to reconnection in the solar corona (Hughes et al. 2003).

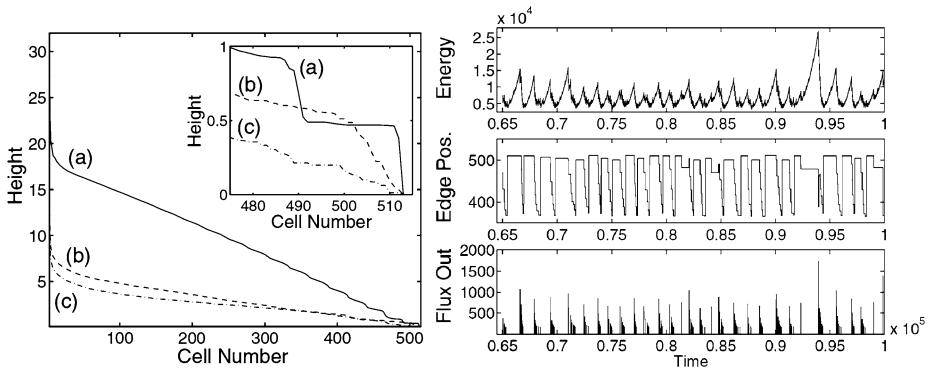


**Fig. 15** Tokamak-like enhanced confinement, edge pedestals, and edge-localized pulses of energy loss in a sandpile model. (*Left*) Time averaged height profiles of a 512-cell sandpile for three different values of the model's sole control parameter; *inset* are edge profiles. (*Right*) Time sequence and magnitude of energy loss events for the corresponding regimes. Reproduced from Chapman et al. (2001a). Copyright (2001) by the American Physical Society

Empirical support for the application of the sandpile paradigm can arise from direct observation of avalanche events in experiments, and in numerical simulations thereof, together with the identification of event statistics that are power law or otherwise strongly non-Gaussian. Such observations are widespread in space and laboratory plasma systems (Dendy and Chapman 2006; Dendy et al. 2007). The primary benefit from the application of the sandpile paradigm arises from the fact that it can model global phenomenology which is otherwise prohibitively difficult to capture or explain. In particular, many real plasmas are complex systems in the technical sense. That is, their global phenomenology emerges from the interaction of multiple plasma physics processes, operating across a very broad range of lengthscales and timescales, coupled nonlinearly together. Examples of global plasma phenomenology, on which the sandpile paradigm sheds light, include: in fusion plasmas (Chapman et al. 2001a, 2001b, 2003; Graves et al. 2002), the existence of different classes of energy confinement regime (Wagner 2007), linked to impulsive energy loss events, see Fig. 15; and in space plasma, the measured distribution of ionospheric current flows that are ultimately driven by impulsive energy release events in the magnetotail (Chapman et al. 1998).

Carreras et al. (1996), Newman et al. (1996) were the first authors to propose a dynamical model to try to explain the extensive experimental evidence of non-diffusive behavior in tokamaks, notably in the so-called *L*-mode discharges. This regime of operation is characterized by very stiff profiles, whose shape is rather independent of the location of the heating sources, and in which superdiffusive propagation of hot and cold pulses is usually observed. They conjectured that the plasma profiles (of pressure, density and temperature) were probably lying in the neighborhood of their critical values for the onset of instabilities, pushed there by the constant external heating. In such a near-marginal state, it is not rare that modes excited at a certain position can propagate radially, in an avalanche-like manner, as the transport induced by the local turbulence suppresses it by flattening the local profile at the price of steepening the profiles in neighbor locations, that can in turn go unstable and propagate the avalanche. In this way, the radial transport in the tokamak in these plasmas acts very much like the sandpile used to propose the concept of self-organized criticality in the 1980s (Bak et al. 1987).

Multiple simulations of plasma turbulence in near-marginal conditions have indeed exhibited this behavior since the seminal work by Carreras et al. (1996). There, the statistics of the avalanches observed were studied, and it was found that they exhibited strong power-laws, very reminiscent of those reported by Bak et al. (1987) in their sandpile studies. More recently, del-Castillo-Negrete et al. (2004b) showed, using the propagator method sketched in Sect. 2, that the radial propagators obtained for tracers in near-marginal cylindrical interchange turbulence clearly exhibited non-Gaussian shape ( $\alpha \sim 0.75$ ) and superdiffusive behavior ( $H \sim 0.66$ ). Consistent with these results, Mier et al. (2008) showed that the statistics of Lagrangian radial displacements in cylindrical dissipative-trapped-electron plasma turbulence also exhibited strong non-Gaussian statistics ( $\alpha \sim 1$ ) and superdiffusive behavior ( $H \sim 0.75$ ).

More recently, it has also been discovered that non-diffusive transport may occur in fusion plasmas whose profiles have gradients that are well above marginal values. This requires the existence of a strongly radially-sheared, poloidal flow. These poloidal flows are frequently self-induced by the turbulence via the Reynolds stresses, and contribute to limit the amplitude of the turbulent fluctuations by taking energy from them and reducing the radial size of turbulent eddies. Although this behavior had been known for some time, it had been assumed that the net effect of the presence of these flows on transport was to reduce the effective transport coefficients, thus improving plasma confinement. Sanchez et al. (2008) showed, however, that the presence of these radially-sheared poloidal flows causes a selection of the sign of the axial vorticity which is consistent with the sign of the shear of the flow. The dynamical consequence of this symmetry breaking is that transport is not only reduced, but its nature also changes into a subdiffusive character. That is, Hurst exponents obtained with the propagator method in this situation consistently yield values  $H < 0.5$  in the radial direction. The values of  $H$  are smaller as the shear in the poloidal flow decreases. Simultaneously, transport along the poloidal direction becomes superdiffusive. The simultaneous observation of subdiffusion and superdiffusion in perpendicular directions is actually common, and has also been observed in other situations. In addition to radial subdiffusion, transport across these radially-sheared poloidal flows can also exhibit Lévy-like statistics. They can be linked to a predator-prey interaction between turbulent fluctuations and the local flow shear, which can translate into radial avalanches in spite of the fact that the overall transport remains subdiffusive (Sanchez et al. 2011).

## 7 Implications of Nonclassical Transport for Astrophysical Plasmas

As shown above, nondiffusive transport has direct consequences for the confinement of laboratory plasmas. In a similar way, the fact that energetic particles in space can propagate superdiffusively has a number of consequences. For instance, solar energetic electrons are usually considered to propagate either diffusively or “scatter-free” (Lin 1974), i.e., in a ballistic way. However, superdiffusive propagation is also a possibility, and this influences both the time of arrival of solar energetic particles, as well as their time profile (Lin 2005; Perri and Zimbardo 2008b). A relevant application is that of particle acceleration at shocks: indeed, the most popular acceleration theory is the so called diffusive shock acceleration (DSA), which assumes normal diffusion (Fisk and Lee 1980; Dosch and Shalchi 2010). One of the most important results of DSA is the spectral index  $s$  of the particle differential energy spectrum, which for relativistic energies reads as

$$s = \frac{r + 2}{r - 1} \quad (19)$$

where  $r = V_1/V_2$  is the compression ratio at the shock, and  $V_1$  and  $V_2$  are the upstream and the downstream plasma speeds, respectively. This theory has been extended to the case of nondiffusive transport by Duffy et al. (1995) and by Kirk et al. (1996). They were motivated by the possibility of subdiffusive transport, corresponding to compound diffusion described by Eq. (16), in the case of a nearly perpendicular shock. In particular, Kirk et al. (1996) have shown that the energy spectral index of DSA is modified in the case of non-diffusive transport, and that the change depends essentially on the scaling properties of the propagator. For instance, in the case of normal diffusion one has the Gaussian propagator, and the scaling variable is  $\xi = x/\sqrt{4Dt}$ . Duffy et al. (1995) and Kirk et al. (1996) were concerned mainly with subdiffusion with  $\gamma < 1$ , so that  $\xi = x/(kt)^{\gamma/2}$ . In the case of superdiffusion described by a Lévy random walk, the propagator has power-law tails and the scaling variable is  $\xi = x/(kt)^{1/(\mu-1)}$  (Zumofen and Klafter 1993),  $k$  being a constant with proper physical dimensions. A superdiffusive shock acceleration (SSA) scenario has been proposed by Perri and Zimbardo (2012), who have shown that in such a case the spectral index of the differential energy spectrum for relativistic particles is given by

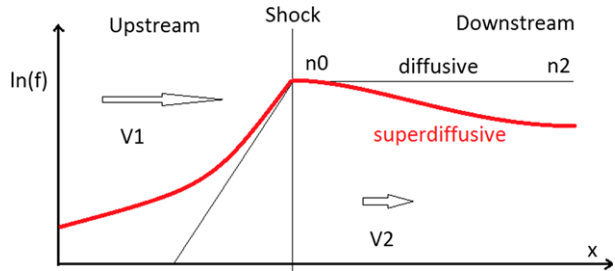
$$s = \frac{6}{r-1} \frac{2-\gamma}{3-\gamma} + 1 \quad (20)$$

and for nonrelativistic particles is given by

$$s = \frac{3}{r-1} \frac{2-\gamma}{3-\gamma} + 1. \quad (21)$$

This spectral index recovers that of DSA in the limit of normal diffusion,  $\gamma = 1$ . Notice that, while the spectral index in Eq. (19) depends only on the compression ratio of the shock, the one obtained in the framework of SSA also depends on the exponent of the mean square particle displacement. Therefore, spectral indices smaller than those of DSA can be obtained for  $\gamma > 1$ . In other words, the assumption of superdiffusive propagation allows one to explain the observation of very hard spectra for relativistic electrons at shell type supernova remnants (Perri and Zimbardo 2012), as well as the harder-than-DSA spectrum observed for MeV ions by the LECP onboard Voyager 2 at the heliospheric termination shock (Decker et al. 2008). Indeed, Decker et al. (2008) find a differential flux spectral index  $s_J$  of about 1.25 (the flux is proportional to the particle velocity, and for nonrelativistic particle this yield an extra  $-0.5$  in the flux spectra index). Assuming the compression ratio  $r = 2$ , obtained by the Plasma Science Instrument, a spectral index  $s_J = s - 0.5 = 2$  is obtained from DSA. To recover the observed spectral index, a compression ratio of 3 would be required by DSA. On the other hand, there is substantial uncertainty on the observed compression ratio: taking into account the solar wind speed decrease observed roughly forty days before the Voyager 2 termination shock crossing and using a two fluid model which considers the energetic particle momentum flux, too, Florinski et al. (2009) have obtained a compression ratio of about 2.4. Therefore it is possible to find a better agreement between the spectral index observed at the termination shock and that foreseen by shock acceleration assuming  $r = 2.4$  and the spectral index in Eq. (21) obtained for nonrelativistic particles by SSA. Using the superdiffusion exponent  $\gamma \sim 1.3 \pm 0.07$  reported by Perri and Zimbardo (2009b) at the termination shock, a differential flux spectral index of  $1.38 \pm 0.2$  is obtained, in reasonable agreement with the Voyager 2 observations when the error bars are taken into account. Since different particle species can exhibit different transport properties (as shown in Perri and Zimbardo 2007, 2008a), this suggests that the energy spectra, too, can be characterized by different indices depending on the particle species considered. For instance,

**Fig. 16** Comparison between the particle distribution function  $f$  spatial profiles for particles accelerated at a shock, in the case of normal diffusion (black line) and in the case of superdiffusion (red line)



the recent PAMELA observations of Galactic cosmic rays show that hydrogen and helium ions have slightly different spectral indices (Adriani et al. 2011), which could be due to different transport regimes.

In addition, one has a change of perspective for the density profile of energetic particles accelerated at the shock, see Fig. 16. That is, while normal diffusion leads to an exponential decay upstream of the shock and to a constant density downstream, superdiffusion leads to a power-law decay upstream and to a far downstream density  $n_2$  which is lower than the density at the shock  $n_0$ . The possible occurrence of this class of density profile should also be investigated in the observational data, both in space and in astrophysical shocks.

Another observable effect was considered by Ragot and Kirk (1997) for the propagation of relativistic electrons away from Coma cluster of galaxies. As the electrons are transported away from the source they cool, and the spectrum softens. In particular, the expected spatial dependence of the spectral index is sensitive to the kind of transport regime. Assuming that the effects of particle acceleration are negligible in the outer part of the Coma cluster, Ragot and Kirk (1997) find that superdiffusion can reproduce the observed rapid softening of the spectrum with distance.

## 8 Conclusions

In this review we have examined some attributes of nondiffusive transport and wave–particle interactions in both laboratory and space plasmas. We have considered the statistical description of anomalous diffusion, based on non-Gaussian random walks and long-range correlations, as well as the use of fractional transport equations. We have also illustrated the results of a number of numerical simulations, describing wave–particle interactions in the kinetic regime, and particle or plasma transport in the presence of electric and magnetic turbulence. These simulations show that nondiffusive transport can be found in many different plasmas. These include laboratory devices for plasma confinement, electron and ion transport in solar coronal loops, and energetic particle transport in the solar wind. Experimental indications of superdiffusion are found for the propagation of particles accelerated at interplanetary shocks, as in the case of co-rotating interaction regions and coronal mass ejections, and for the propagation of relativistic electrons in the Coma cluster. Avalanching transport in toroidal plasmas and superdiffusive acceleration at shocks has also been described.

We have discussed in some detail the suprathreshold ion dynamics in the SMT configuration of the TORPEX device. Although this configuration is relatively simple, it contains all the basic elements for suprathreshold ion dynamics in a number of physical systems. The framework established through study of the SMT scenario can be used for interpreting suprathreshold ion dynamics in fusion devices with high-energy neutral beams and alpha particle production, cosmic ray propagation, and solar wind interaction with the magnetosphere.

Moreover, we expect that the results presented herein are relevant to suprathermal ion dynamics in other basic plasma physics configurations, where superdiffusive and subdiffusive ion transport have recently been measured (Zhou et al. 2010, 2011), and in magnetically confined plasmas, where it may be possible to model the interaction of energetic particles with Alfvénic turbulence using the Lévy walk approach.

The examples considered show that nonclassical transport is fundamental to the most important problems in plasma physics, ranging from plasma confinement in toroidal fusion devices to energetic particle propagation and acceleration in space plasmas. Therefore, understanding the microphysics of nonclassical transport is a high priority across a variety of plasmas.

**Acknowledgements** This work was part-funded by the RCUK Energy Programme under grant EP/I501045 and the European Communities under the contract of Association between EURATOM and CCFE. The views and opinions expressed herein do not necessarily reflect those of the European Commission. The TORPEX experiments and simulations were supported in part by the Swiss National Science Foundation. The authors wish to acknowledge the valuable support of the CRPP technical team. K.G. was supported by US-NSF IRFP grant OISE-0853498. The hybrid Vlasov-Maxwell numerical simulations discussed in the present work were performed on the Fermi supercomputer at Cineca (Bologna, Italy), within the project ASWTURB 2011 (HP10BO2REM), supported by the Italian Super-computing research allocation (ISCRA), and within the European project PRACE Pra04-771 (Partnership for advanced computing in Europe). D.P. is supported by the Italian Ministry for University and Research (MIUR) PRIN 2009 funds (grant number 20092YP7EY). G.Z. acknowledges support from the European Union FP7, Marie Curie project 269198 – Geoplasmas. S. P.’s research has been supported by “Borsa Post-doc POR Calabria FSE 2007/2013 Asse IV Capitale Umano - Obiettivo Operativo M.2”.

## References

- S. Abdullaev, Structure of motion near saddle points and chaotic transport in Hamiltonian systems. *Phys. Rev. E* **62**, 3508 (2000)
- O. Adriani et al. (PAMELA collaboration), PAMELA measurements of cosmic-ray proton and helium spectra. *Science* **332**, 69 (2011)
- O. Alexandrova, J. Saur, C. Lacombe et al., Universality of the solar wind turbulent spectrum from MHD to electron scales. *Phys. Rev. Lett.* **103**, 165003 (2009)
- F. Anderegg, C.F. Driscoll, D.H. Dubin et al., Electron acoustic waves in pure ion plasmas. *Phys. Plasmas* **16**, 055705 (2009)
- S.V. Annibaldi, G. Manfredi, R.O. Dendy et al., Evidence for strange kinetics in Hasegawa-Mima turbulent transport. *Plasma Phys. Control. Fusion* **42**, L13 (2000)
- S.V. Annibaldi, G. Manfredi, R.O. Dendy, Non-Gaussian transport in strong plasma turbulence. *Phys. Plasmas* **9**, 791 (2002)
- J.A. Araneda, E. Marsch, A.F. Viñas, Proton core heating and beam formation via parametrically unstable Alfvén-cyclotron waves. *Phys. Rev. Lett.* **100**, 125003 (2008)
- J.A. Araneda, Y. Maneva, E. Marsch, Preferential heating and acceleration of  $\alpha$  particles by Alfvén-cyclotron waves. *Phys. Rev. Lett.* **102**, 175001 (2009)
- P. Bak, C. Tang, K. Wiesenfeld, Self-organized criticality: an explanation of  $1/f$  noise. *Phys. Rev. Lett.* **59**, 381 (1987)
- P. Bak, C. Tang, K. Wiesenfeld, Self-organized criticality. *Phys. Rev. A* **38**, 364 (1988)
- S.D. Bale, P.J. Kellogg, F.S. Mozer et al., Measurement of the electric fluctuation spectrum of magnetohydrodynamic turbulence. *Phys. Rev. Lett.* **94**, 215002 (2005)
- J.W. Bieber, W.H. Matthaeus, C.W. Smith, Proton and electron mean free paths: the Palmer consensus revisited. *Astrophys. J.* **420**, 294 (1994)
- C.K. Birdsall, A.B. Langdon, *Plasma Physics via Computer Simulation* (McGraw-Hill, New York, 1985)
- R. Bitane, G. Zimbardo, P. Veltri, Electron transport in coronal loops: the influence of the exponential separation of magnetic field lines. *Astrophys. J.* **719**, 1912 (2010)
- S. Bourouaine, E. Marsch, F.M. Neubauer, Correlations between the proton temperature anisotropy and transverse high frequency waves in the solar wind. *Geophys. Res. Lett.* **37**, L14104 (2010)
- S. Bourouaine, E. Marsch, F.M. Neubauer, On the relative speed and temperature ratio of solar wind alpha particles and protons: collisions versus wave effects. *Astrophys. J.* **728**, L3 (2011a)

- S. Bourouaine, E. Marsch, F.M. Neubauer, Temperature anisotropy and differential streaming of solar wind ions. Correlations with transverse fluctuations. *Astron. Astrophys.* **536**, A39 (2011b)
- A. Bovet, A. Fasoli, I. Furno et al., Investigation of fast ion transport in TORPEX. *Nucl. Fusion* **52**, 094017 (2012)
- R. Bruno, V. Carbone, The solar wind as a turbulence laboratory. *Living Rev. Sol. Phys.* **2**, 4 (2005)
- G.S. Burillo, B.P. van Milligen, A. Thyagaraja, Analysis of the radial transport of tracers in a turbulence simulation. *Phys. Plasmas* **16**, 042319 (2009)
- E. Camporeale, D. Burgess, The dissipation of solar wind turbulent fluctuations at electron scales. *Astrophys. J.* **730**, 114 (2011)
- B.A. Carreras, V.E. Lynch, D.E. Newman, A model realization of self-organized criticality for plasma confinement. *Phys. Plasmas* **3**, 2903 (1996)
- S.C. Chapman, N. Watkins, R.O. Dendy et al., A simple avalanche model as an analogue for magnetospheric activity. *Geophys. Res. Lett.* **25**, 2397 (1998)
- S.C. Chapman, R.O. Dendy, G. Rowlands, A sandpile model with dual scaling regimes for laboratory, space and astrophysical plasmas. *Phys. Plasmas* **6**, 4169 (1999)
- S.C. Chapman, R.O. Dendy, B. Hnat, A sandpile model with tokamak-like enhanced confinement phenomenology. *Phys. Rev. Lett.* **86**, 2814 (2001a)
- S.C. Chapman, R.O. Dendy, B. Hnat, A simple avalanche model for astrophysical and laboratory confinement systems. *Phys. Plasmas* **8**, 1969 (2001b)
- S.C. Chapman, R.O. Dendy, B. Hnat, Self organisation of edge and internal pedestals in a sandpile. *Plasma Phys. Control. Fusion* **45**, 301 (2003)
- C.H.K. Chen, A. Mallet, T.A. Yousef et al., Anisotropy of Alfvénic turbulence in the solar wind and numerical simulations. *Mon. Not. R. Astron. Soc.* **415**, 3219 (2011)
- R.-B. Decker, S.M. Krimigis, E.C. Roelof et al., Mediation of the solar wind termination shock by non-thermal ions. *Nature* **454**, 67 (2008)
- D. del-Castillo-Negrete, Asymmetric transport and non-Gaussian statistics of passive scalars in vortices in shear. *Phys. Fluids* **10**, 576 (1998)
- D. del-Castillo-Negrete, B.A. Carreras, V.E. Lynch, Fractional diffusion in plasma turbulence. *Phys. Plasmas* **11**, 3854 (2004a)
- D. del-Castillo-Negrete, B.A. Carreras, V.E. Lynch, Nondiffusive transport in plasma turbulence: a fractional diffusion approach. *Phys. Rev. Lett.* **94**, 065003 (2004b)
- R.O. Dendy, P. Helander, Sandpiles, silos and tokamak phenomenology: a brief review. *Plasma Phys. Control. Fusion* **39**, 1947 (1997)
- R.O. Dendy, P. Helander, On the appearance and non-appearance of self-organised criticality in sandpiles. *Phys. Rev. E* **57**, 3641 (1998)
- R.O. Dendy, P. Helander, M. Tagger, On the role of self-organised criticality in accretion systems. *Astron. Astrophys.* **337**, 962 (1998)
- R.O. Dendy, S.C. Chapman, Characterisation and interpretation of strongly nonlinear phenomena in fusion, space, and astrophysical plasmas. *Plasma Phys. Control. Fusion* **48**, B313 (2006)
- R.O. Dendy, S.C. Chapman, M. Paczuski, Fusion, space, and solar plasmas as complex systems. *Plasma Phys. Control. Fusion* **49**, A95 (2007)
- J.M. Dewhurst, B. Hnat, R.O. Dendy, The effects of nonuniform magnetic field strength on density flux and test particle transport in drift wave turbulence. *Phys. Plasmas* **16**, 072306 (2009)
- J.M. Dewhurst, B. Hnat, R.O. Dendy, Finite Larmor radius effects on test particle transport in drift wave-zonal flow turbulence. *Plasma Phys. Control. Fusion* **52**, 025004 (2010). doi:[10.1088/0741-3335/52/2/025004](https://doi.org/10.1088/0741-3335/52/2/025004)
- A. Diallo, A. Fasoli, I. Furno et al., Dynamics of plasma blobs in a shear flow. *Phys. Rev. Lett.* **101**, 115005 (2008)
- P.H. Diamond, S.-I. Itoh, T.S. Hahm, Zonal flows in plasmas—a review. *Plasma Phys. Control. Fusion* **47**, R35 (2005)
- P.H. Diamond, A. Hasegawa, K. Mima, Vorticity dynamics, drift wave turbulence, and zonal flows: a look back and a look ahead. *Plasma Phys. Control. Fusion* **53**, 124001 (2011)
- A. Dosch, A. Shalchi, Diffusive shock acceleration at interplanetary perpendicular shock waves: influence of the large scale structure of turbulence on the maximum particle energy. *Adv. Space Res.* **46**, 1208 (2010)
- P. Duffy, J.-G. Kirk, Y.-A. Gallant et al., Anomalous transport and particle acceleration at shocks. *Astron. Astrophys.* **302**, L21 (1995)
- A. Fasoli, B. Labit, M. McGrath et al., Electrostatic turbulence and transport in a simple magnetized plasma. *Phys. Plasmas* **13**, 055902 (2006)
- A. Fasoli, A. Burckel, L. Federspiel et al., Electrostatic instabilities, turbulence and fast ion interactions in the TORPEX device. *Plasma Phys. Control. Fusion* **52**, 124020 (2010)
- J. Feder, *Fractals* (Plenum, New York, 1988)

- L.A. Fisk, M.A. Lee, Shock acceleration of energetic particles in corotating interaction regions in the solar wind. *Astrophys. J.* **237**, 620 (1980)
- V. Florinski, R.B. Decker, J.A. le Roux et al., An energetic-particle-mediated termination shock observed by Voyager 2. *Geophys. Res. Lett.* **36**, L12101 (2009)
- A. Fujisawa, Experimental studies of mesoscale structure and its interactions with microscale waves in plasma turbulence. *Plasma Phys. Control. Fusion* **53**, 124015 (2011)
- I. Furno, B. Labit, M. Podestà et al., Experimental observation of the blob-generation mechanism from interchange waves in a plasma. *Phys. Rev. Lett.* **100**, 055004 (2008a)
- I. Furno, B. Labit, A. Fasoli et al., Mechanism for blob generation in the TORPEX toroidal plasma. *Phys. Plasmas* **15**, 055903 (2008b)
- I. Furno, M. Spolaore, C. Theiler et al., Direct two-dimensional measurements of the field-aligned current associated with plasma blobs. *Phys. Rev. Lett.* **106**, 245001 (2011)
- S.P. Gary, S. Saito, H. Li, Cascade of whistler turbulence: particle-in-cell simulations. *Geophys. Res. Lett.* **35**, L02104 (2008)
- J. Giacalone, Large-scale hybrid simulations of particle acceleration at a parallel shock. *Astrophys. J.* **609**, 452 (2004)
- J. Giacalone, Cosmic-ray transport and interaction with shocks. *Space Sci. Rev.* (2011). doi:[10.1007/s11214-011-9763-2](https://doi.org/10.1007/s11214-011-9763-2)
- J.P. Graves, R.O. Dendy, K.I. Hopcraft et al., The role of clustering effects in non-diffusive transport in tokamaks. *Phys. Plasmas* **9**, 1596 (2002)
- S. Günter, C. Angioni, M. Apostoliceanu et al., Overview of ASDEX upgrade results—development of integrated operating scenarios for ITER. *Nucl. Fusion* **45**, S98 (2005)
- D.A. Gurnett, E. Marsch, W. Pilipp et al., Ion-acoustic waves and related plasma observations in the solar wind. *J. Geophys. Res.* **84**, 2029 (1979)
- K. Gustafson, D. Del-Castillo-Negrete, W. Dorland, Finite Larmor radius effects on nondiffusive tracer transport in a zonal flow. *Phys. Plasmas* **15**, 102309 (2008)
- K. Gustafson, P. Ricci, A. Bovet et al., Suprathermal ion transport in simple magnetized torus configurations. *Phys. Plasmas* **19**, 062306 (2012a)
- K. Gustafson, P. Ricci, I. Furno et al., Nondiffusive suprathermal ion transport in simple magnetized toroidal plasmas. *Phys. Rev. Lett.* **108**, 035006 (2012b)
- K. Gustafson, P. Ricci, Lévy walk description of suprathermal ion transport. *Phys. Plasmas* **19**, 032304 (2012)
- T. Hauff, F. Jenko, S. Eule, Intermediate non-Gaussian transport in plasma core turbulence. *Phys. Plasmas* **14**, 102316 (2007)
- T. Hauff, F. Jenko, Mechanisms and scalings of energetic ion transport via tokamak microturbulence. *Phys. Plasmas* **15**, 2307 (2008)
- P. Helander, S.C. Chapman, R.O. Dendy et al., Exactly solvable sandpile with fractal avalanching. *Phys. Rev.* **59**, 6356 (1999)
- W.A. Hornsby, A.R. Bell, R.J. Kingham et al., A code to solve the Vlasov Fokker-Planck equation applied to particle transport in magnetic turbulence. *Plasma Phys. Control. Fusion* **52**, 075011 (2010)
- D. Hughes, M. Paczuski, R.O. Dendy et al., Solar flares as cascades of reconnecting magnetic loops. *Phys. Rev. Lett.* **90**, 131101 (2003)
- S. Inagaki, T. Tokuzawa, K. Itoh et al., Observations of long-distance radial correlation in toroidal plasma turbulence. *Phys. Rev. Lett.* **107**, 115001 (2011)
- J.R. Jokipii, Cosmic-ray propagation. I. Charged particles in a random magnetic field. *Astrophys. J.* **146**, 480 (1966)
- J.G. Kirk, P. Duffy, Y.A. Gallant, Stochastic particle acceleration at shocks in the presence of braided magnetic fields. *Astron. Astrophys.* **314**, 1010 (1996)
- J.G. Kirk, R.O. Dendy, Shock acceleration of cosmic rays: a critical review. *J. Phys. G* **27**, 1589 (2001)
- J. Klafter, A. Blumen, M.F. Shlesinger, Stochastic pathway to anomalous diffusion. *Phys. Rev. A* **35**, 3081 (1987)
- A.J. Klimas, J.A. Valdivia, D. Vassiliadis et al., Self-organized criticality in the substorm phenomenon and its relation to localized reconnection in the magnetospheric plasma sheet. *J. Geophys. Res.* **105**(A8), 18765 (2000)
- J. Kóta, J.R. Jokipii, Velocity correlation and the spatial diffusion coefficients of cosmic rays: compound diffusion. *Astrophys. J.* **531**, 1067 (2000)
- J.A. Krommes, C. Oberman, R.B. Kleva, Plasma transport in stochastic magnetic fields. Part 3. Kinetics of test particle diffusion. *J. Plasma Phys.* **30**, 11 (1983)
- B. Labit, C. Theiler, A. Fasoli et al., Blob-induced toroidal momentum transport in simple magnetized plasmas. *Phys. Plasmas* **18**, 032308 (2011)
- P.O. Lagage, C.J. Cesarsky, Cosmic-ray shock acceleration in the presence of self-excited waves. *Astron. Astrophys.* **118**, 223 (1983a)

- P.O. Lagage, C.J. Cesarsky, The maximum energy of cosmic rays accelerated by supernova shocks. *Astron. Astrophys.* **125**, 249 (1983b)
- L.D. Landau, On the vibrations of the electronic plasma. *J. Phys. (Moscow)* **10**, 25 (1946)
- M.A. Lee, L.A. Fisk, Shock acceleration of energetic particles in the heliosphere. *Space Sci. Rev.* **32**, 205 (1982)
- R.E. Lee, S.C. Chapman, R.O. Dendy, Ion acceleration processes at reforming collisionless shocks. *Phys. Plasmas* **12**, 012901 (2005a)
- R.E. Lee, S.C. Chapman, R.O. Dendy, Reforming perpendicular shocks in the presence of pickup protons: initial ion acceleration. *Ann. Geophys.* **23**, 643 (2005b)
- R.P. Lin, Non-relativistic solar electrons. *Space Sci. Rev.* **16**, 189 (1974)
- R.P. Lin, Relationship of solar flare accelerated particles to solar energetic particles (SEPs) observed in the interplanetary medium. *Adv. Space Res.* **35**, 1857 (2005)
- E. Lu, R. Hamilton, Avalanches of the distribution of solar flares. *Astrophys. J.* **380**, L89 (1991)
- F. Mainardi, Y. Luchko, G. Pagnini, The fundamental solution of the space-time fractional diffusion equation. *Fract. Calc. Appl. Anal.* **4**, 153–192 (1996)
- M.A. Malkov, P.H. Diamond, Weak hysteresis in a simplified model of the L-H transition. *Phys. Plasmas* **16**, 012504 (2009)
- B.B. Mandelbrot, J.W. van Ness, Fractional Brownian motions, fractional noises and applications. *SIAM Rev.* **10**, 422 (1968)
- G. Manfredi, R.O. Dendy, Test-particle transport in strong electrostatic drift turbulence with finite Larmor radius effects. *Phys. Rev. Lett.* **76**, 4360 (1996)
- G. Manfredi, M. Shoucri, R.O. Dendy et al., Vlasov gyrokinetic simulations of ion-temperature-gradient driven instabilities. *Phys. Plasmas* **3**, 202 (1996)
- G. Manfredi, R.O. Dendy, Transport properties of energetic particles in a turbulent electrostatic field. *Phys. Plasmas* **4**, 628 (1997)
- G. Manfredi, C.M. Roach, R.O. Dendy, Zonal flow and streamer generation in drift turbulence. *Plasma Phys. Control. Fusion* **43**, 825 (2001)
- A. Mangeney, F. Califano, C. Cavazzoni et al., A numerical scheme for the integration of the Vlasov-Maxwell system of equations. *J. Comput. Phys.* **179**, 405 (2002)
- E. Marsch, K.-H. Mühlhäuser, R. Schwenn et al., Solar wind protons: three-dimensional velocity distributions and derived plasma parameters measured between 0.3 and 1 AU. *J. Geophys. Res.* **87**, A1 (1982a)
- E. Marsch, K.-H. Mühlhäuser, R. Schwenn et al., Solar wind helium ions: observations of the Helios solar probes between 0.3 and 1 AU. *J. Geophys. Res.* **35**, A1 (1982b)
- E. Marsch, Kinetic physics of the solar corona and solar wind. *Living Rev. Sol. Phys.* **3**, 1 (2006)
- J.A. Mier, R. Sanchez, L. Garcia et al., Characterization of non-diffusive transport in plasma turbulence via a novel Lagrangian method. *Phys. Rev. Lett.* **101**, 165001 (2008)
- J.A. Miller, Particle acceleration in impulsive solar flares. *Space Sci. Rev.* **86**, 79 (1998)
- E.W. Montroll, G.H. Weiss, Random walks on lattices. II. *J. Math. Phys.* **6**, 167 (1965)
- S.H. Müller, A. Diallo, A. Fasoli et al., Plasma blobs in a basic toroidal experiment: origin, dynamics, and induced transport. *Phys. Plasmas* **14**, 110704 (2007)
- D.E. Newman, B.A. Carreras, P.H. Diamond et al., The dynamics of marginality and self-organized criticality as a paradigm for turbulent transport. *Phys. Plasmas* **3**, 1858 (1996)
- T.N. Parashar, S. Servidio, B. Breech et al., Kinetic driven turbulence: structure in space and time. *Phys. Plasmas* **17**, 102304 (2010)
- T.N. Parashar, S. Servidio, M.A. Shay et al., Effect of driving frequency on excitation of turbulence in a kinetic plasma. *Phys. Plasmas* **18**, 092302 (2011)
- S. Perri, G. Zimbardo, Evidence of superdiffusive transport of electrons accelerated at interplanetary shocks. *Astrophys. J.* **671**, L177 (2007)
- S. Perri, F. Lepreti, V. Carbone et al., Position and velocity space diffusion of test particles in stochastic electromagnetic fields. *Europhys. Lett.* **78**, 40003 (2007)
- S. Perri, G. Zimbardo, Superdiffusive transport of electrons accelerated at corotating interaction regions. *J. Geophys. Res.* **113**, A03107 (2008a). doi:[10.1029/2007JA012695](https://doi.org/10.1029/2007JA012695)
- S. Perri, G. Zimbardo, Observations of anomalous transport of energetic electrons in the heliosphere. *Astrophys. Space Sci. Trans.* **4**, 27 (2008b)
- S. Perri, G. Zimbardo, Ion and electron superdiffusive transport in the interplanetary space. *Adv. Space Res.* **44**, 465 (2009a)
- S. Perri, G. Zimbardo, Ion superdiffusion at the solar wind termination shock. *Astrophys. J.* **693**, L118 (2009b)
- S. Perri, G. Zimbardo, A. Greco, On the energization of protons interacting with 3-D time-dependent electromagnetic fields in the Earth's magnetotail. *J. Geophys. Res.* **116**, A05221 (2011). doi:[10.1029/2010JA016328](https://doi.org/10.1029/2010JA016328)

- S. Perri, G. Zimbardo, Superdiffusive shock acceleration. *Astrophys. J.* **750**, 87 (2012)
- D. Perrone, F. Valentini, P. Veltri, The role of alpha particles in the evolution of the solar-wind turbulence toward short spatial scales. *Astrophys. J.* **741**, 43 (2011)
- D. Perrone, F. Valentini, S. Servidio, S. Dalena, P. Veltri, Vlasov simulations of multi-ion plasma turbulence in the solar wind. *Astrophys. J.* **762**, 99 (2013)
- G. Plyushchev, A. Diallo, A. Fasoli et al., Fast ion source and detector for investigating the interaction of turbulence with suprathermal ions in a low temperature toroidal plasma. *Rev. Sci. Instrum.* **77**, 10F503 (2006)
- M. Podestà, A. Fasoli, B. Labit et al., Cross-field transport by instabilities and blobs in a magnetized toroidal plasma. *Phys. Rev. Lett.* **101**, 045001 (2008)
- P. Pommois, P. Veltri, G. Zimbardo, Anomalous and Gaussian transport regimes in anisotropic three-dimensional magnetic turbulence. *Phys. Rev. E* **59**, 2244 (1999)
- P. Pommois, P. Veltri, G. Zimbardo, Field line diffusion in solar wind magnetic turbulence and energetic particle propagation across heliographic latitudes. *J. Geophys. Res.* **106**, 24965 (2001)
- P. Pommois, G. Zimbardo, P. Veltri, Anomalous, non-Gaussian transport of charged particles in anisotropic magnetic turbulence. *Phys. Plasmas* **14**, 012311 (2007)
- G. Qin, W.H. Matthaeus, J.W. Bieber, Subdiffusive transport of charged particles perpendicular to the large scale magnetic field. *Geophys. Res. Lett.* **29**, 1048 (2002a). doi:[10.1029/2001GL014035](https://doi.org/10.1029/2001GL014035)
- G. Qin, W.H. Matthaeus, J.W. Bieber, Perpendicular transport of charged particles in composite model turbulence: recovery of diffusion. *Astrophys. J.* **578**, L117 (2002b)
- B.R. Ragoth, J.G. Kirk, Anomalous transport of cosmic ray electrons. *Astron. Astrophys.* **327**, 432 (1997)
- D.V. Reames, Particle acceleration at the Sun and in the heliosphere. *Space Sci. Rev.* **90**, 413 (1999)
- A.B. Rechester, M.N. Rosenbluth, Electron heat transport in a Tokamak with destroyed magnetic surfaces. *Phys. Rev. Lett.* **40**, 38 (1978)
- P. Ricci, C. Theiler, A. Fasoli et al., Langmuir probe-based observables for plasma-turbulence code validation and application to the TORPEX basic plasma physics experiment. *Phys. Plasmas* **16**, 055703 (2009)
- P. Ricci, B.N. Rogers, Transport scaling in interchange-driven toroidal plasmas. *Phys. Plasmas* **16**, 062303 (2009)
- P. Ricci, B.N. Rogers, Turbulence phase space in simple magnetized toroidal plasmas. *Phys. Rev. Lett.* **104**, 145001 (2010)
- P. Ricci, C. Theiler, A. Fasoli et al., Methodology for turbulence code validation: quantification of simulation-experiment agreement and application to the TORPEX experiment. *Phys. Plasmas* **18**, 032109 (2011)
- D. Ruffolo, W.H. Matthaeus, P. Chuychai, Trapping of solar energetic particles by the small-scale topology of solar wind turbulence. *Astrophys. J.* **597**, L169 (2003)
- F. Sahrhadi, M.L. Goldstein, G. Belmont et al., Three dimensional anisotropic  $k$  spectra of turbulence at subproton scales in the solar wind. *Phys. Rev. Lett.* **105**, 131101 (2010)
- S. Saito, S.P. Gary, H. Li et al., Whistler turbulence: particle-in-cell simulations. *Phys. Plasmas* **15**, 102305 (2008)
- G. Samorodnitsky, M.S. Taqqu, *Stable Non-Gaussian Distributions* (Chapman & Hall, New York, 1994)
- R. Sanchez, B.A. Carreras, B. van Milligen, Fluid limits of nonintegrable CTRWs in terms of fractional differential equations. *Phys. Rev. E* **71**, 011111 (2005)
- R. Sanchez, B.A. Carreras, D.E. Newman et al., Renormalization of tracer turbulence leading to fractional differential equations. *Phys. Rev. E* **74**, 016305 (2006)
- R. Sanchez, D.E. Newman, J.-N. Leboeuf et al., Nature of transport across sheared zonal flows in electrostatic ion-temperature-gradient gyrokinetic plasma turbulence. *Phys. Rev. Lett.* **101**, 205002 (2008)
- R. Sanchez, D.E. Newman, J.-N. Leboeuf et al., Nature of turbulent transport across sheared zonal flows: insights from gyrokinetic simulations. *Plasma Phys. Control. Fusion* **53**, 074018 (2011)
- H. Schmitz, S.C. Chapman, R.O. Dendy, Electron pre-acceleration mechanisms in the foot region of high Alfvénic Mach number shocks. *Astron. Astrophys.* **579**, 327 (2002b)
- H. Schmitz, S.C. Chapman, R.O. Dendy, The influence of electron temperature and magnetic field on cosmic ray injection at high Mach number shocks. *Astron. Astrophys.* **570**, 637 (2002a)
- S. Servidio, F. Valentini, F. Califano et al., Local kinetic effects in two-dimensional plasma turbulence. *Phys. Rev. Lett.* **108**, 045001 (2012)
- A. Shalchi, I. Kourakis, A new theory for perpendicular transport of cosmic rays. *Astron. Astrophys.* **470**, 405 (2007)
- A. Shalchi, Applicability of the Taylor-Green-Kubo formula in particle diffusion theory. *Phys. Rev. E* **83**, 046402 (2011)
- M.F. Shlesinger, J. Klafter, Y.M. Wong, Random walks with infinite spatial and temporal moments. *J. Stat. Phys.* **27**, 499 (1982)
- W.J. Shugart, H. Reiss, Transient nucleation in H<sub>2</sub>O–H<sub>2</sub>SO<sub>4</sub> mixtures: a stochastic approach. *J. Chem. Phys.* **65**, 2827 (1976)

- T. Sugiyama, D. Shiota, Sign for super-diffusive transport of energetic ions associated with a coronal-mass-ejection-driven interplanetary shock. *Astrophys. J.* **731**, L34 (2011)
- R.C. Tautz, Simulation results on the influence of magneto-hydrodynamic waves on cosmic ray particles. *Plasma Phys. Control. Fusion* **52**, 045016 (2010)
- R.C. Tautz, A. Shalchi, On the diffusivity of cosmic ray transport. *J. Geophys. Res.* **115**, A03104 (2010). doi:[10.1029/2009JA014944](https://doi.org/10.1029/2009JA014944)
- C. Theiler, A. Diallo, A. Fasoli et al., The role of the density gradient on intermittent cross-field transport events in a simple magnetized toroidal plasma. *Phys. Plasmas* **15**, 042303 (2008)
- C. Theiler, I. Furno, P. Ricci et al., Cross-field motion of plasma blobs in an open magnetic field line configuration. *Phys. Rev. Lett.* **103**, 065001 (2009)
- G.R. Tynan, A. Fujisawa, G. McKee, A review of experimental drift turbulence studies. *Plasma Phys. Control. Fusion* **51**, 113001 (2009)
- F. Valentini, P. Veltri, A. Mangeney, A numerical scheme for the integration of the Vlasov–Poisson system of equations, in the magnetized case. *J. Comput. Phys.* **210**, 730 (2005)
- F. Valentini, P. Trávníček, F. Califano et al., A hybrid-Vlasov model based on the current advance method for the simulation of collisionless magnetized plasma. *J. Comput. Phys.* **225**, 753 (2007)
- F. Valentini, P. Veltri, F. Califano et al., Cross-scale effects in solar-wind turbulence. *Phys. Rev. Lett.* **101**, 025006 (2008)
- F. Valentini, P. Veltri, Electrostatic short-scale termination of solar-wind turbulence. *Phys. Rev. Lett.* **102**, 225001 (2009)
- F. Valentini, F. Califano, P. Veltri, Two-dimensional kinetic turbulence in the solar wind. *Phys. Rev. Lett.* **104**, 205002 (2010)
- F. Valentini, F. Califano, D. Perrone et al., New ion-wave path in the energy cascade. *Phys. Rev. Lett.* **106**, 165002 (2011a)
- F. Valentini, F. Califano, D. Perrone et al., Excitation of nonlinear electrostatic waves with phase velocity close to the ion-thermal speed. *Plasma Phys. Control. Fusion* **53**, 105017 (2011b)
- F. Valentini, D. Perrone, P. Veltri, Short-wavelength electrostatic fluctuations in the solar wind. *Astrophys. J.* **739**, 54 (2011c)
- B.Ph. van Milligen, R. Sanchez, B.A. Carreras, Probabilistic finite-size transport models for fusion: anomalous transport and scaling laws. *Phys. Plasmas* **11**, 2272 (2004)
- F. Wagner, A quarter-century of H-mode studies. *Plasma Phys. Control. Fusion* **49**, B1 (2007)
- N.W. Watkins, S.C. Chapman, R.O. Dendy et al., Robustness of collective behaviour in strongly driven avalanche models: magnetospheric implications. *Geophys. Res. Lett.* **26**, 2617 (1999)
- N.W. Watkins, M.P. Freeman, S.C. Chapman et al., Testing the SOC hypothesis for the magnetosphere. *J. Atmos. Sol.-Terr. Phys.* **63**, 1435 (2001)
- G.M. Webb, G.P. Zank, E.Kh. Kaghshvili et al., Compound and perpendicular diffusion of cosmic rays and random walk of the field lines. I. Parallel particle transport models. *Astrophys. J.* **651**, 211 (2006)
- T. Yamada, S.-I. Itoh, T. Maruta et al., Anatomy of plasma turbulence. *Nat. Phys.* **4**, 721 (2008)
- G.M. Zaslavsky, Chaos, fractional kinetics, and anomalous transport. *Phys. Rep.* **371**, 461 (2002)
- S. Zhou, W.W. Heidbrink, H. Boehmer et al., Turbulent transport of fast ions in the large plasma device. *Phys. Plasmas* **17**, 092103 (2010)
- S. Zhou, W.W. Heidbrink, H. Boehmer et al., Dependence of fast-ion transport on the nature of the turbulence in the large plasma device. *Phys. Plasmas* **18**, 082104 (2011)
- G. Zimbardo, P. Veltri, P. Pommois, Anomalous, quasilinear, and percolative regimes for magnetic-field-line transport in axially symmetric turbulence. *Phys. Rev. E* **61**, 1940 (2000a)
- G. Zimbardo, A. Greco, P. Veltri, Superballistic transport in tearing driven magnetic turbulence. *Phys. Plasmas* **7**, 1071 (2000b)
- G. Zimbardo, P. Pommois, P. Veltri, Magnetic flux tube evolution in solar wind anisotropic magnetic turbulence. *J. Geophys. Res.* **109**, A02113 (2004). doi:[10.1029/2003JA010162](https://doi.org/10.1029/2003JA010162)
- G. Zimbardo, Anomalous particle diffusion and Lévy random walk of magnetic field lines in three-dimensional solar wind turbulence. *Plasma Phys. Control. Fusion* **47**, B755 (2005)
- G. Zimbardo, P. Pommois, P. Veltri, Superdiffusive and subdiffusive transport of energetic particles in solar wind anisotropic magnetic turbulence. *Astrophys. J.* **639**, L91 (2006)
- G. Zimbardo, R. Bitane, P. Pommois et al., Kolmogorov entropy of magnetic field lines in the percolation regime. *Plasma Phys. Control. Fusion* **51**, 015005 (2009)

- G. Zimbardo, A. Greco, L. Sorriso-Valvo et al., Magnetic turbulence in the geospace environment. *Space Sci. Rev.* **156**, 89 (2010)
- G. Zimbardo, S. Perri, P. Pommois et al., Anomalous particle transport in the heliosphere. *Adv. Space Res.* **49**, 1633 (2012)
- G. Zumofen, A. Blumen, J. Klafter et al., Lévy-walks for turbulence: a numerical study. *J. Stat. Phys.* **54**, 1519 (1989)
- G. Zumofen, J. Klafter, Scale-invariant motion in intermittent chaotic systems. *Phys. Rev. E* **47**, 851 (1993)